nature COMMUNICATIONS

ARTICLE

Received 18 Nov 2015 | Accepted 3 Aug 2016 | Published 23 Sep 2016

DOI: 10.1038/ncomms12818 OPEN

Low-oxygen waters limited habitable space for early animals

R. Tostevin[1,†], R.A. Wood[2], G.A. Shields[1], S.W. Poulton[3], R. Guilbaud[4], F. Bowyer[2], A.M. Penny[2], T. He[1], A. Curtis[2], K.H. Hoffmann[5] & M.O. Clarkson[2,6]

The oceans at the start of the Neoproterozoic Era (1,000–541 million years ago, Ma) were dominantly anoxic, but may have become progressively oxygenated, coincident with the rise of animal life. However, the control that oxygen exerted on the development of early animal ecosystems remains unclear, as previous research has focussed on the identification of fully anoxic or oxic conditions, rather than intermediate redox levels. Here we report anomalous cerium enrichments preserved in carbonate rocks across bathymetric basin transects from nine localities of the Nama Group, Namibia (~550–541 Ma). In combination with Fe-based redox proxies, these data suggest that low-oxygen conditions occurred in a narrow zone between well-oxygenated surface waters and fully anoxic deep waters. Although abundant in well-oxygenated environments, early skeletal animals did not occupy oxygen impoverished regions of the shelf, demonstrating that oxygen availability (probably >10 μM) was a key requirement for the development of early animal-based ecosystems.

[1] Department of Earth Sciences, University College London, Gower Street, London WC1E 6BT, UK. [2] School of GeoSciences, The University of Edinburgh, James Hutton Road, Edinburgh EH9 3FE, UK. [3] School of Earth and Environment, University of Leeds, Leeds LS2 9JT, UK. [4] Department of Earth Sciences, University of Cambridge, Downing Street, Cambridge CB2 3EQ, UK. [5] Geological Survey of Namibia, Private Bag 13297, Windhoek, Namibia. [6] Department of Chemistry, University of Otago, Dunedin 9054, New Zealand. † Present address: Department of Earth Sciences, University of Oxford, Oxford OX1 3AN, UK. Correspondence and requests for materials should be addressed to R.T. (email: Rosalie.tostevin@earth.ox.ac.uk).

Geochemical proxies based on Fe-S-C and trace metal systematics have been widely used to reconstruct the progressive oxygenation of the oceans during the Neoproterozoic and Cambrian[1–7]. Accumulating evidence indicates that the deep oceans were dominantly anoxic and ferruginous (Fe containing) throughout most of the Precambrian, with euxinic (sulfidic) mid-depth waters prevalent along continental margins from ~1.8 to 1.0 billion years ago (Ga)[1,6,8]. From ~1.0 to 0.58 Ga, however, euxinic mid-depth waters became less prevalent and ferruginous conditions expanded, with oxic conditions still largely restricted to surface waters[1,8,9]. The oxygenation of the deeper marine realm was both protracted and spatially heterogeneous, with some marine basins recording persistent deep-water oxygenation from ~580 Ma, whereas regional anoxia remained a feature of some deeper shelf environments into the Cambrian, ~520 Ma (refs 4,5,7,10) and beyond.

The course of Neoproterozoic oxygenation, and cause and effect associations with the appearance of animals, remains controversial[4,11–13]. Although modern soft-bodied sponge-grade animals may tolerate oxygen concentrations as low as 1.25–10 μM[14], new innovations in the late Ediacaran, such as motility[15], the rise of predation and skeletonization[16–18], are all hypothesized to have required higher levels of oxygen[19]. However, the oxygen demands of early animals are unconstrained and observations from modern biota cannot necessarily be applied to early animals of unknown affinity. Furthermore, although soft-bodied and skeletal Ediacaran fauna dominantly occur in sediments interpreted to have been deposited from oxic waters, fossil occurrences have also been reported in sediments characterized by anoxic geochemical signals[5,20]. In the latter case, this may be because some early complex organisms were able to colonize habitats during fleeting periods of oxia (such short-lived oxygenation is difficult to detect by geochemical proxies that tend to integrate relatively long periods of time). In both of the above cases, however, there is uncertainty as to whether early animal evolution occurred under fully oxygenated conditions or whether intermediate redox conditions were more prevalent, which by extension suggests that the oxygen requirements of more complex organisms were lower[3,14]. An in-depth understanding of these links is currently hampered by the inability of most redox proxies to distinguish between fully oxygenated and intermediate redox states, including nitrogenous or manganous conditions, which may overlap with low concentrations of oxygen[21,22]. Indeed, it is possible that 'oxic' horizons identified through Fe and trace element geochemistry may in fact have formed under low-oxygen conditions (but not fully anoxic), at levels insufficient to support diverse skeletal animal communities.

In oxic environments, Ce(III) is oxidized to insoluble Ce(IV) and preferentially scavenged relative to the rest of the rare earth elements and yttrium, REY[23]. The standard reduction potential of Ce(IV) (+1.61°V) is closer to Mn(IV) (+1.23°V) than Fe(III) (+0.77°V) and Ce oxidation is catalysed on the surface of Mn (oxyhydr)oxides[24]. Therefore, the redox cycling of Ce in seawater is closely related to Mn(II)/Mn(IV) transformations, which occur at a higher redox potential than the Fe(II)/Fe(III) couple, and hence Mn cycling is more sensitive to intermediate redox conditions[23–26]. Ce anomalies (Ce_{SN}/Ce^{*}_{SN}) are calculated here based on relative enrichments or depletions in shale-normalized Ce ($[Ce]_{SN}$) compared with neighbouring non-redox sensitive REY:

$$Ce_{SN}/Ce^{*}_{SN} = \frac{[Ce]_{SN}}{([Pr]_{SN})^{2}/[Nd]_{SN}} \quad (1)$$

Owing to the accumulation of Ce(IV) on the surface of Mn (oxyhydr)oxides, oxic seawater becomes Ce depleted and exhibits a negative Ce anomaly (<0.9)[23]. These Mn (oxyhydr)oxides may be buried intact in sediments beneath oxic bottom waters, or may dissolve in the water column if they encounter low-oxygen waters,

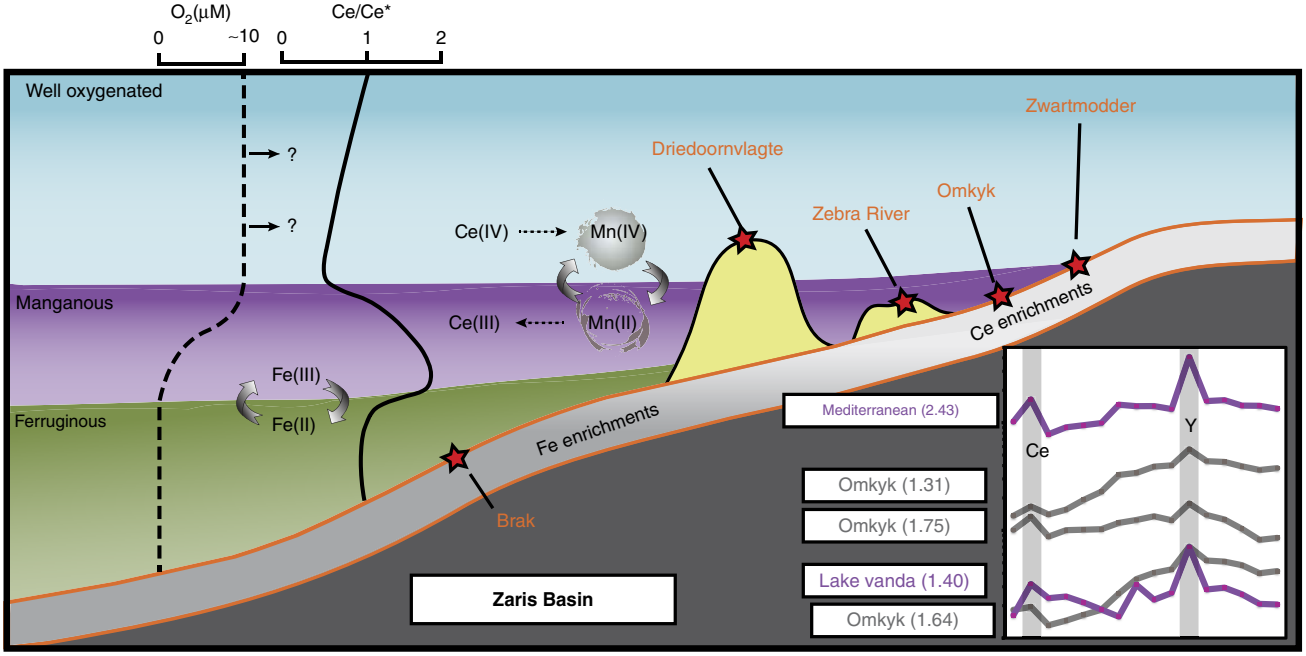

Figure 1 | Schematic representation of redox zones and associated geochemical signals. Generalized redox conditions across the Zaris Basin, Nama Group, during a highstand systems tract. Positive Ce anomalies form as Mn (oxyhydr)oxides dissolve in the manganous zone and Fe enrichments form under anoxic ferruginous conditions. Ten micromole is an estimate of O_2 concentrations in the manganous zone, but overlying well-oxygenated waters probably contained higher O_2 concentrations. Representative REY patterns, including positive Ce anomalies (magnitude in brackets), are shown for the Omkyk section in the Nama Group, alongside manganous zones from two modern environments[25,27] (modern water column data plotted as [REY] × 10^6 for easy comparison with sedimentary [REY]).

releasing excess Ce. Therefore, waters beneath the Mn(IV)/Mn(II) redoxcline commonly exhibit a positive Ce anomaly (>1.3)[25–27]. Positive Ce anomalies have been recorded alongside Mn enrichments in some modern waters, including Lake Vanda, Antarctica (Ce_{SN}/Ce^{*}_{SN} up to 2.3, Fig. 1)[25], in anoxic brines in the eastern Mediterranean (Ce_{SN}/Ce^{*}_{SN} up to 2.43, Fig. 1)[27] and in the deep-marine Cariaco Basin (Ce_{SN}/Ce^{*}_{SN} up to 1.21)[26].

Water column REY and associated Ce anomalies are thought to be preserved in non-skeletal carbonate rocks without fractionation[28]. Carbonate-bound REY are relatively robust to diagenetic alteration[28] and dolomitization[29], but any alteration of the Ce anomaly can be identified using non-redox sensitive REY anomalies, such as the Y/Ho ratio, which would also be altered away from seawater patterns[30,31]. Sequential dissolution methods enable REY in the carbonate phase to be isolated, preventing contributions from sedimentary (oxyhydr)oxides or clays[31], which would carry a non-seawater signature.

In the present study, we measured REY in 259 carbonate rocks of the Nama Group from nine sites across two basins. The majority of samples are very pure calcites with low siliciclastic components, but where samples are partially dolomitized they have been treated differently during leaching[31]. The resulting REY data have been screened for traditional seawater features (Y/Ho ratios >67) and samples with evidence for diagenetic alteration or contributions from non-carbonate phases have been excluded from the presented Ce/Ce* data (see Methods). We additionally use redox interpretations based on published Fe speciation data for these carbonate samples[5]. Fe speciation distinguishes anoxic from oxic water column conditions through enrichments in highly reactive Fe (Fe_{HR}) relative to total Fe (Fe_T)[1,32]. Anoxic enrichments in Fe_{HR} occur due to the water column formation of either pyrite under euxinic conditions[32] or non-sulfidized Fe_{HR} minerals (such as Fe oxides or carbonates) under anoxic ferruginous conditions[1] (see Methods). We interpret ususual Ce enrichments across the Nama Group to indicate Mn-rich, low-oxygen conditions, supported by additional redox information from Fe-based proxies on the same samples. This enables us to distinguish fully anoxic, intermediate and well-oxygenated waters across a shelf-to-basin transect and compare these with the distribution of early skeletal animal life.

Results

Geological setting. The succession was deposited ~550–541 Ma broadly coincident with the first appearance of skeletal animals[16–18], as well as trace fossil evidence for motility[15] and soft-bodied fossils belonging to the Ediacaran biota[33]. Our samples cover a range of palaeo depths from shallow inner ramp to deeper outer ramp waters, in the Kanies, Omkyk and Hoogland Members of the Kuibis Subgroup, and the Spitzkopf and Feldschuhorn Members of the upper Schwarzrand Subgroup[5,16] (Fig. 2, Supplementary Table 1 and also see Supplementary Note 1 for full details of the geological setting). We focus on the first known skeletal animals, *Cloudina*, a globally distributed eumetazoan of possible cnidarian affinity[17,34,35]; *Namacalathus*, interpreted as a stem group eumetaozan[36] or triploblast lophophorate[37] and reported from multiple localities; and *Namapoikia*, an encrusting possible cnidarian or poriferan known only from the Nama Group[18].

Ce anomaly interpretation. In the Nama Group, the majority of REY distribution patterns are smooth and show a flat or light REY-depleted shape on shale-normalized plots, positive La anomalies, low total rare earth elements (REE) concentrations and superchondritic Y/Ho ratios (>67), all of which indicate preservation and extraction of original seawater signals (see Supplementary Note 2 and supplementary Figs 1–10 for a description of all data). Four samples exhibit negative Ce anomalies (<0.9; Fig. 2), consistent with an oxic water column interpretation obtained for these samples from Fe speciation[5]. Ce anomalies are, as expected, absent from the persistently anoxic and ferruginous deepest water setting[5] (Fig. 2). However, significant positive Ce anomalies (1.30–2.15) are prevalent in inner ramp sections in both sub-basins (64 samples). In six cases, positive Ce anomalies are associated with anoxic ferruginous signals and in one case a positive Ce anomaly is associated with a sample that gives a robust oxic Fe_{HR}/Fe_T signal. However, for the majority of samples (~90%), Fe_T was <0.5 wt%, preventing a robust evaluation of water column redox conditions from Fe speciation alone. In these cases, samples have elevated Mn/Fe ratios (median = 0.39), when compared with samples with no positive Ce anomalies (median = 0.14) and anoxic ferruginous samples (median = 0.10), which provides an independent constraint on water column redox conditions, as discussed below (Fig. 3).

The regionally widespread positive Ce anomalies across the Zaris and Witputs Basins of the Nama Group imply a surplus of Ce sustained by a rain down of Mn (oxyhydr)oxides from shallow oxygenated surface waters and this is supported by the elevated Mn/Fe ratios of these samples (Fig. 3). Redox cycling of Mn (oxyhydr)oxides across the Mn(IV/II) redoxcline would leave ambient waters locally enriched in the Ce released during Mn(IV) reduction (Fig. 1). We therefore interpret positive Ce anomalies (>1.3) to indicate intermediate manganous conditions (Table 1 and also see Supplementary Discussion for alternative Ce enrichment mechanisms). Where there is an absence of both positive Ce anomalies and any indication of enrichment in Fe (that is, $Fe_{HR}/Fe_T<0.22$ or $Fe_T<0.5$ wt%), we suggest that bottom waters were probably well oxygenated (which is consistent with Fe_{HR}/Fe_T signals in interbedded siliciclastics[5]), thus preventing the onset of both Fe and Mn reduction. Where data are equivocal (for example, Fe_{HR}/Fe_T between 0.22–0.38 and no Ce anomaly), we are unable to interpret redox conditions.

Positive Ce anomalies have not been widely reported from carbonate-rich sediments, but there are limited examples from iron formation[38] and cherts[39] in the earlier Paleozoic. Positive Ce anomalies, between 1.3 and 2.2, are also reported for late Ediacaran dolomites, from just a few samples in the possibly contemporaneous Krol Formation of northern India[40]. If these data were demonstrated to preserve seawater REY patterns, this strengthens the data from the Nama Group and hints that manganous conditions may have been a common feature of Ediacaran oceanic margins. By contrast, demonstrably contemporaneous terminal Ediacaran Ce anomaly data from the Yangtze platform, South China, show increasing Ce depletion towards the Ediacaran–Cambrian Boundary, indicating progressive oxygenation of the local marine environment[41]. Ce anomalies record local redox conditions and thus independent signals would be expected both within and between marine basins.

Redox conditions in the Nama group. The outer ramp was persistently anoxic and ferruginous (Brak section), and animals are absent from these settings[5] (Fig. 4). The deep inner-ramp sections show periods of anoxic ferruginous, manganous and well-oxygenated conditions (Zebra River and Omkyk sections). In these settings, animals are notably absent from ferruginous and manganous waters, whereas well-oxygenated waters support abundant skeletal animals, up to 35 mm in diameter, and adjacent localities show trace fossil evidence for motility[15]. The shallowest inner ramp sections show high-frequency temporal fluctuations

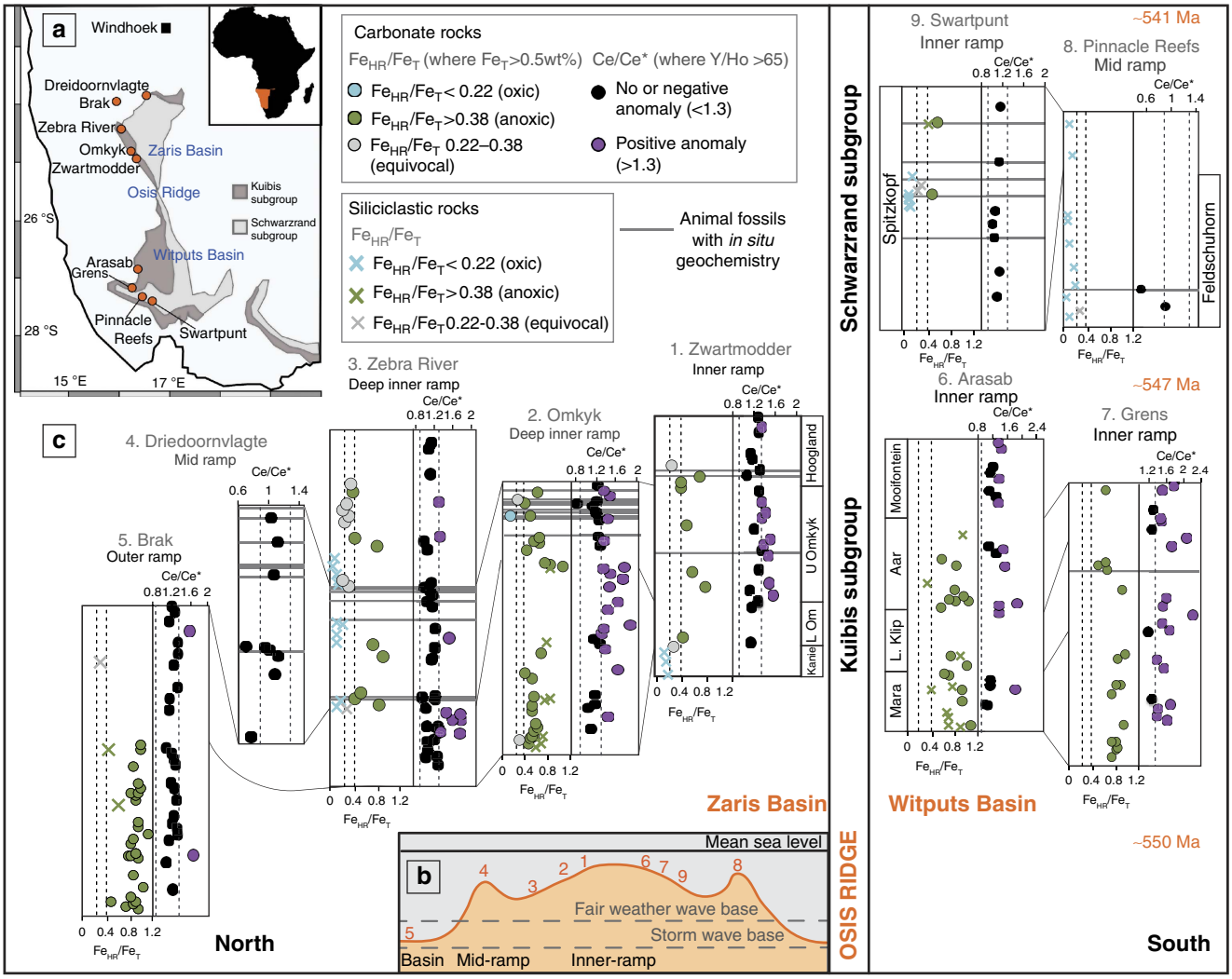

Figure 2 | Summary of Ce_{SN}/Ce^*_{SN} and Fe-speciation data for nine localities. The location of nine sections within the Kuibis and Schwarzrand Subgroups of the Nama Group is shown on a simplified geological map of Namibia[52,53,55,57] (**a**), as well as on a schematic cross-section, indicating average relative water depth (**b**). The numbers along the basin profile relate to the relative position of each section as numbered in **c**. Fe_{HR}/Fe_T data for each location is shown for carbonate and siliciclastic rocks[5], alongside Ce_{SN}/Ce^*_{SN} data, screened for carbonate rocks showing seawater REY patterns (for example, molar Y/Ho > 67) (**c**). Blue Fe_{HR}/Fe_T data indicate where Fe speciation predicts oxic conditions[5] and positive Ce anomalies indicate where waters are interpreted to have been manganous. The presence of *in situ* biota is noted by grey lines[5].

between anoxic ferruginous, manganous and well-oxygenated conditions (Zwartmodder, Arasab and Grens sections), as might be expected due to fluctuations in the depth of the chemocline (Fig. 4). At Zwartmodder, skeletal animals are present in thin beds[5], but there is only one skeletal horizon at Grens and no animal fossils at Arasab.

In contrast to these ecologies, the Driedoornvlagte pinnacle reef grew within a transgressive systems tract in a mid-ramp position, which was persistently well-oxygenated and hosts some very large skeletal animals[5,18] (up to 1 m) and complex reef-building ecologies[17]. In the younger Schwarzrand Subgroup, which extends close to the Ediacaran–Cambrian Boundary (~547–541 Ma), there is evidence for persistent well-oxygenated conditions[5] and mid-ramp Pinnacle Reefs host mixed communities of large and small skeletal animals. At Swartpunt, abundant burrows and soft-bodied biota occur in siliciclastic horizons, where Fe speciation indicates oxic conditions[5], whereas small *in-situ* skeletal animals are found in carbonate rocks throughout the succession[5].

Discussion

Our geochemical and palaeontological data demonstrate a striking relationship between the precise redox condition of the water column and the presence and abundance of evidence for animal life. Constraints from the modern open ocean suggest that dissolved Mn(II), and therefore Ce(III), can start to build up in low concentrations in oxic waters with dissolved $O_2 < 100\,\mu M$[22]. However, manganous conditions, whereby Mn becomes the dominant redox buffer, are achieved at lower oxygen concentrations. Reduced Mn can remain stable in the presence of up to 10 μM O_2 (refs 21,42), although Mn oxidation has been reported locally at lower O_2 concentrations where oxidation is catalysed by enzymatic processes[43]. Thus, active Mn cycling can occur in anoxic waters, but is commonly documented in partially oxic waters with at least 10 μM O_2 (and up to 100 μM O_2; Fig. 1)[21,42,44,45], which represents significant oxygen depletion in comparison with modern fully oxygenated surface waters (~250 μM O_2). The reduction potential for Ce is higher than that for Mn and so the 10 μM O_2 constraint for manganous

waters may represent a lower limit on Ce cycling, as sufficient O_2 to oxidize both Ce and Mn is required for the formation of Ce anomalies.

Our multi-proxy approach allows us to distinguish between fully anoxic and intermediate waters, which contained low but significant amounts of oxygen. Where Fe speciation in Ce-enriched samples gives a robust anoxic signal ($Fe_{HR}/Fe_T > 0.38$), Mn reduction may have persisted, but conditions must have been fully anoxic. However, the majority of samples interpreted to be manganous have insufficient Fe_T for Fe speciation (with 85% of these falling below 0.25 wt% Fe_T and 35% falling below 0.1 wt% Fe_T). Even very low oxygen concentrations (nM) are sufficient to prevent Fe_{HR} enrichments and thus the low Fe_T in shallower environments across the Nama Group may be indicative of oxic conditions[46], and this is supported by persistent oxic Fe_{HR}/Fe_T ratios obtained from interbedded siliciclastics in some sections[5]. We therefore suggest that the manganous zone occurred between well-oxygenated surface waters and deeper anoxic, ferruginous waters, commonly overlapping with low but significant concentrations of oxygen (at least ~10 μM; Fig. 1).

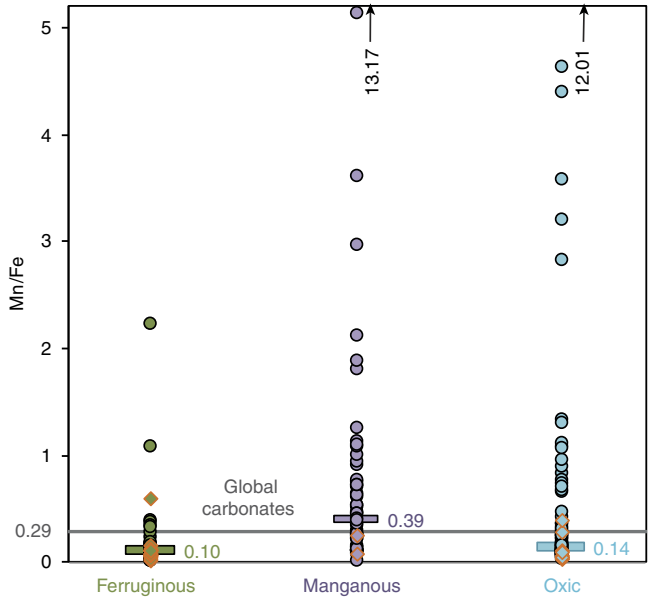

Figure 3 | Average Mn/Fe ratios under different redox conditions. Mn/Fe ratios for samples identified as manganous (positive Ce/Ce* and low Fe_T or oxic Fe-speciation signals), ferruginous (anoxic Fe-speciation signals) and oxic (oxic Fe-speciation signals, no positive Ce anomaly). Mn/Fe is enriched in manganous samples compared with global carbonate (0.29; ref. 70). Bars represent median values. Red outlines indicate dolomitized samples. Arrows indicate samples with exceptionally high Mn/Fe ratios that lie above the limit of the *y* axis.

Oxygen exerts an important control on ecosystem structure in modern environments, whereby low-oxygen environments are inhabited by smaller animals often lacking skeletons and forming low-diversity communities with simple food webs[19]. In general, skeletons are absent from modern oxygen minimum zones when O_2 drops below 13 μM and large animals are often absent below 45 μM (refs 47,48). However, the importance of oxygen in supporting early animal ecosystems as they became increasingly complex in form, metabolic demand and behaviour through the Ediacaran Period is currently unresolved[2,3,5,11–13]. In the Nama Group the majority of small skeletal animals (>75%) and all evidence for large skeletal animals, motility, soft-bodied biota and complex or long-lived ecologies[17] are found in sediments deposited from well-oxygenated waters (Fig. 4). The identification of low-oxygen, manganous water column conditions thus provides a compelling explanation for the general absence of biota in these settings and implies that poorly oxygenated conditions were insufficient to meet the relatively high oxygen requirements of these early skeletal animals[5,15,17,33]. If we take an upper O_2 limit for Mn and Ce reduction of 10 μM O_2, this suggests that Mn-enriched waters could theoretically support small, soft-bodied animals such as sponges[14]. In contrast, the absence of skeletal animals in Mn-enriched waters is consistent with the high energetic cost of skeletonization. Possible biomarkers for sponge animals appear in the fossil record at >635 Ma (ref. 49), but it is possible that the availability of well-oxygenated habitats was necessary to support the later appearance of skeletonization, at ~550 Ma. However, it is also unlikely to be that reaching an oxygenation threshold alone is sufficient to explain the appearance of skeletons[50] and many have argued that the trigger for the rise of skeletonization may have been ecological, such as the rise of predation[17,36,51].

Our approach highlights that intermediate redox conditions were probably widespread in the Ediacaran ocean, but have not previously been appreciated due to the inability of most commonly used proxies to identify such conditions. Our data suggest that low-oxygen water column conditions were insufficient to support early skeletal and reef-building animals, and thus the extent of suitable habitat space may have been less than previously identified. The widespread radiation of skeletal animals during the subsequent Cambrian explosion may have been facilitated by a global rise in the extent of habitable, oxygenated seafloor[7], alongside other genetic and ecological factors. Our data therefore yield new insight into the debate on the role of oxygen in early animal evolution, suggesting that well-oxygenated waters were necessary to support the appearance of the skeletal animals and complex ecologies that are typical of the terminal Neoproterozoic.

Table 1 | Framework for co-interptetation of Ce_{SN}/Ce_{SN}^* and Fe-speciation data on the same samples.

	Ce anomaly		
Fe-speciation	**Negative anomaly**	**Equivocal (no anomaly)**	**Positive anomaly**
Anoxic $Fe_{HR}/Fe_T > 0.38$, $Fe_{py}/Fe_{HR} < 0.7$	NA	Ferruginous	Ferruginous
Equivocal Fe_{HR}/Fe_T 0.22–0.38	Oxic	Unknown	Manganous
Oxic $Fe_{HR}/Fe_T < 0.22$, $Fe_T < 0.5$wt% (likely to be oxic)	Oxic	Oxic	Manganous

Fe_{HR}, highly reactive Fe; Fe_T, total Fe; NA, not applicable.

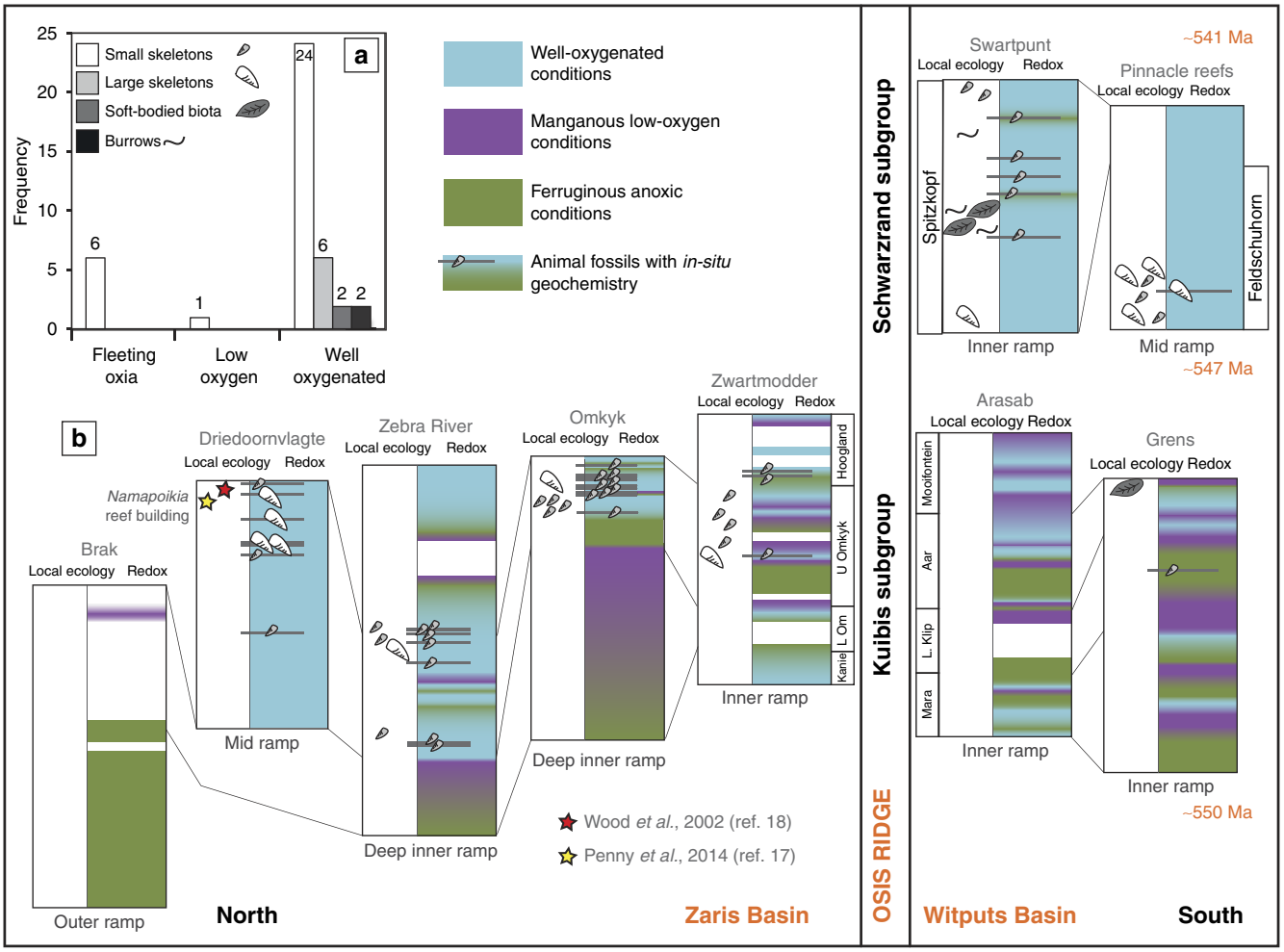

Figure 4 | Integrated redox interpretations compared with local ecology. A comprehensive redox interpretation is shown for each of the nine localities in the Nama Group, determined using combined Fe and Ce signals. *In situ* fossils (grey lines), and local ecologies[5] and general ecology from the literature[17,18] are shown alongside local water column redox conditions (**b**). The bar chart plots the frequency that different biota are found in each redox zone[5] (**a**). Large skeletal fossils and burrows are found exclusively in well-oxygenated settings and small skeletal fossils are largely restricted to well-oxygenated conditions, but may occur where conditions were only fleetingly oxic.

Methods

Geological context and sample quality. The Nama Group is a well-preserved terminal Neoproterozoic carbonate and siliciclastic sequence, ranging from upper shore-line/tidal flats to below-wave-base lower shoreface, deposited in a ramp system ~550–541 Ma (refs 5,16,52–55). Samples from nine shelf-to-basin sections within the Zaris and Witputs basins of the Nama Group encompass a range of palaeo-depths from outer- to inner-ramp settings (Supplementary Table 1). Stratigraphic correlations are well-established based on sequence boundaries and ash beds[5,16]. The age of the upper Nama Group is relatively well-constrained from U-Pb dating of three ash beds within the group, including one at 548.8 ± 1 Ma in the Hoogland Member of the Kuibis Subgroup[54], revised to 547.32 ± 0.31 Ma (ref. 56). The base of the Nama Group is diachronous, but is between 553 and 548 Ma. The Proterozoic–Cambrian boundary is represented by a regionally extensive erosional unconformity near the top of the Schwarzrand Subgroup in the southern Basin[53,54,57,58], which is overlain by incised-valley fill dated (U-Pb on an ashbed) at 539 ± 1 Ma (ref. 54). Therefore, the Nama Group section spans at least 7 Myr and extends to within 2 Myr of the Ediacaran–Cambrian Boundary[52].

Unweathered samples were selected and powdered or drilled avoiding alteration, veins or weathered edges. For Zebra River section, powders were drilled from thin section counterparts, targeting fine-grained cements. Carbonate rocks in the Nama Group are very pure, but they have all undergone pervasive recrystallization. Less than 15% of the samples in this study are dolomitized and there is no petrographic evidence for deep burial dolomitization in the Nama Group[5,55].

Samples were logged for fossil occurrences and sampled within established sequence stratigraphic frameworks, using detailed sedimentology[5,52,53] (see Supplementary Notes 1 and 2). The presence of different forms of skeletal biota, soft-bodied biota and trace fossils are reported for precise horizons where geochemical analyses have been performed[5], indicated by grey lines in Figs 2 and 3. General local ecology, supported by additional information from the literature, is also marked, without associated grey lines. Our sampling focused on carbonates and hence skeletal fossils are over-represented compared with soft-bodied biota and trace fossils. We define 'large' skeletal animals as >10 mm in any dimension, which includes *Cloudina hartmannae*, some *Namacalathus* and *Namapoikia*.

Rare earth elements in carbonate rocks. Rare earth elements and yttrium (REY) have a predictable distribution pattern in seawater and non-biological carbonate rocks should preserve local water column REY at the sediment–water interface[28]. Ce anomalies develop progressively, but cutoff values are established to define negative and positive anomalies. We define a negative anomaly as $Ce_{SN}/Ce^{*}_{SN} < 0.9$, consistent with previous work[59]. A positive anomaly, using the same reference frame, would be defined as $Ce_{SN}/Ce^{*}_{SN} > 1.1$. However, as positive anomalies are not previously described from carbonate sediments, we cautiously use a higher cutoff, $Ce_{SN}/Ce^{*}_{SN} > 1.3$, to ensure any positive anomalies are environmentally significant with respect to positive anomalies recorded from some modern manganous waters (1.21–2.43) (see Supplementary Note 3 and Supplementary Fig 11 for discussion of Ce_{SN}/Ce^{*}_{SN} cutoffs). Although positive or negative Ce anomalies in carbonate rocks probably represent seawater redox conditions, the absence of any Ce anomaly (0.9–1.3) is somewhat equivocal and could result from anoxic water column conditions or overprinting of any Ce anomaly during diagenesis or leaching[31]. Alternately, Ce anomaly formation may be disrupted in surface waters because of wind-blown dust or photo-reduction of Mn oxides[60]. Fe (oxyhydr)oxides may also be REY carriers, but do not contain the clear Ce enrichments observed in Mn (oxyhydr)oxides (see Supplementary Note 4 for discussion of the role of Fe (oxyhydr)oxides in REY cycling).

Diagenetic phosphates, Fe and Mn (oxyhydr)oxides, organic matter and clays can potentially affect the REY signatures of authigenic sedimentary rocks if they are

partially dissolved during the leaching process[61–63]. Care has been taken to partially leach samples, to isolate the carbonate phase without leaving excess acid, which may leach contaminant phases (see ref. 31 for detailed discussion of methodology). Powdered calcite samples were cleaned in Milli-Q water and pre-leached in 2% nitric acid, to remove adsorbed and easily exchangeable ions associated with clay minerals. The remaining sample was partially leached, also in 2% (w/v) nitric acid, to avoid contributions from contaminant phases such as oxides and clays[31]. The supernatant was removed from contact with the remaining residue, diluted with 2% nitric acid and analysed via inductively coupled plasma mass spectrometry in the Cross-Faculty Elemental Analysis Facility, University College London. This leaching method has been designed to extract the carbonate-bound REY pool without contributions from (oxyhydr)oxides or clays[31]. These same leachates were also analysed for major element concentrations (Mg, Fe, Mn, Al and Sr) via inductively coupled plasma optical emission spectrometry. Oxide interference was monitored using the formation rate of Ce oxide and the formation of 2+ ions was monitored using Ba^{2+}. All REY concentrations were normalized to post-Archean Australian Shale.

Standard solutions analysed after every ten samples were within 5% of known concentrations. Replicate analyses on the inductively coupled plasma mass spectrometry give a relative s.d. <5% for most trace elements, with a larger s.d. for the heavy REE that sometimes have non-normalized concentrations <0.5 p.p.b. Carbonate standard material CRM 1c was prepared using the same leaching procedure as the samples and repeat analyses give a relative s.d. <5% for individual REY concentrations, and calculated Ce anomalies (average = 0.80) give a relative s.d. <3%.

Mn/Sr ratios are <1 for the majority (97%) of samples and δ^{18}Ocarb is > −10‰, indicating minimal open-system elemental and isotopic exchange during diagenesis, and excluding deep burial dolomitization (Supplementary Fig. 12). Ce anomaly data are only presented for carbonates that preserve seawater REY features (smooth patterns with molar Y/Ho > 67)[28,31], indicating they originate from the carbonate portion of the whole rock, without contributions from detrital or oxide phases. For samples with Y/Ho > 67, 85% also have ∑REE <2 p.p.m. and all have ∑REE <10 p.p.m. La anomalies, and small positive Eu and Gd enrichments are prevalent in samples with Y/Ho > 67 (Supplementary Fig. 11 and Supplementary Note 5 for discussion of Y anomaly thresholds). Positive Ce anomalies are associated with low Mn/Sr ratios (<1) and low Al, Zr, Ti, Fe and Mn contents in the leachate (<0.2 wt% for Fe and <500 p.p.m. for Mn), indicating minimal contamination due to diagenetic exchange, leaching of clays or Fe–Mn (oxyhydr)oxide phases (Supplementary Fig. 12).

Rare earth elements in shales. Shales from throughout the Zebra River section, including inter-reef deposits and lateral subordinate shales between grainstone horizons, were fully digested using HNO_3-HF-$B(OH)_3$-$HClO_4$ at the University of Leeds. These full digestions include the dominant siliciclastic component, but would also encompass any subordinate (oxyhydr)oxide phases, organic matter or carbonate components. The full digestions were dried down, washed twice in 50% nitric acid and resuspended in 2% nitric acid for analysis on an inductively coupled plasma mass spectrometry in the Cross-Faculty Elemental Analysis Facility, University College London.

Relative to standardized shale composition, post-Archean Australian Shale[64], the Zebra River shales show consistent patterns (Supplementary Fig. 13), with middle-REY enrichment (bell-shaped index = 1.25) and negative Y anomalies (shale-normalized Y/Ho = 0.88), but no anomalous Ce behaviour. These patterns resemble those reported for Fe (oxyhydr)oxides[65,66] and may well derive in part from the high Fe_{ox} contents of these shales (up to 1.2%). Shales carry a 'continental-type' REY pattern and represent a baseline from which surface-solution fractionation of REY begins, and thus they are commonly used to normalize seawater REY patterns.

Fe speciation in carbonates and siliciclastics. The Fe speciation method quantifies Fe that is (bio)geochemically available in surficial environments (termed Fe_{HR}) relative to Fe_T. Mobilization and subsequent precipitation of Fe in anoxic water column settings results in Fe_{HR} enrichments in the underlying sediment. The nature of anoxia (that is, sulfide-rich or Fe-containing) is determined by the extent of sulfidation of the Fe_{HR} pool[1]. Fe speciation data for carbonate rock samples discussed here and accompanying interbedded siliciclastic rocks come from previously published data[5]. The Fe-speciation technique was performed using well-established sequential extraction schemes[1,67]. The method targets operationally defined Fe pools, including carbonate-associated-Fe (Fe_{Carb}), ferric oxides (Fe_{Ox}), magnetite (Fe_{Mag}), pyrite Fe (Fe_{Py}) and Fe_T. Fe_{HR} is defined as the sum of Fe_{carb} (extracted with Na-acetate at pH 4.5 and 50 °C for 48 h), Fe_{ox} (extracted via Na-dithionite at pH 4.8 for 2 h), Fe_{mag} (extracted with ammonium oxalate for 6 h) and Fe_{py} (calculated from the mass of sulfide extracted during $CrCl_2$ distillation). Fe_T extractions were performed on ashed samples (8 h at 550 °C) using HNO_3-HF-H_3BO_3-$HClO_4$. All Fe concentrations were measured via atomic absorption spectrometry and replicate extractions gave a relative s.d. of <4% for all steps, leading to <8% for calculated Fe_{HR}. Fe_{Py} was calculated from the wt% of sulfide extracted as Ag_2S using hot Cr(II)Cl_2 distillation[68]. A boiling HCl distillation before the Cr(II)Cl_2 distillation ruled out the potential presence of acid volatile sulfides in our samples. Pyrite extractions give reproducibility for Fe_{py} of 0.005 wt%, confirming high precision for this method. Analysis of a certified reference material (PACS-2, $Fe_T = 4.09 \pm 0.07$ wt%, $n = 4$; certified value = 4.09 ± 0.06 wt%) confirms that our method is accurate. Replicate analyses ($n = 6$) gave a precision of ± 0.06 wt% for Fe_T and a relative s.d. of <5% for the Fe_{HR}/Fe_T ratio.

Calibration in modern and ancient marine environments suggests that $Fe_{HR}/Fe_T < 0.22$ indicates deposition under oxic water column conditions, whereas $Fe_{HR}/Fe_T > 0.38$ indicates anoxic conditions[1]. Ratios between 0.22–0.38 are considered equivocal and may represent either oxic or anoxic depositional conditions. For sediments identified as anoxic, $Fe_{py}/Fe_{HR} > 0.8$ is diagnostic for euxinic conditions and $Fe_{py}/Fe_{HR} < 0.7$ defines ferruginous deposition[1]. Although originally calibrated for siliciclastics[1,32], enrichments in Fe_{HR}/Fe_T can also be identified in carbonates deposited under anoxic water column conditions[69]. These Fe_{HR} enrichments can far exceed Fe_{HR} contents expected under normal oxic deposition, where trace amounts (~0.1 wt%) of Fe may be incorporated into carbonates, or precipitate as Fe–Mn coatings[69]. However, although early dolomitization in shallow burial environments does not generally cause a significant increase in Fe_{HR}, late-stage deep-burial dolomitization may significantly increase Fe_{HR}[69], but there is no petrographic evidence for deep-burial dolomitization in our samples[5,16]. Consistent with a recent calibration[69], we have limited the application of Fe speciation to carbonate samples with >0.5 wt% Fe_T, which buffers against the impact of non-depositional enrichments in Fe_{HR}[69]. Where Fe_T is very low (<0.5wt%), this may indicate deposition under oxic conditions[69]. In addition, however, we stress that all of our redox interpretations based on Fe speciation in carbonates are entirely consistent with data from siliciclastic horizons interbedded with and/or associated with carbonate rocks contained within the same m- to dm-scale depositional cycle[5].

Equivocal Fe_{HR}/Fe_T ratios could be a consequence of dilution of a high water column Fe_{HR} flux through rapid sedimentation[32] (for example, in turbidite settings) or post-depositional transformation of unsulfidized Fe_{HR} minerals to less reactive sheet silicate minerals[8,67]. Further, local Fe_{HR} enrichments can occur due to preferential trapping of Fe_{HR} in inner shore or shallow marine environments (for example, flood plains, salt marshes, deltas and lagoons). However, none of the presented Fe_{HR} data here are from rocks that show evidence of turbiditic deposition and are from dominantly open marine settings. Oxidative weathering may result in mineralogical transformation of Fe minerals. Oxidation of siderite would transfer Fe_{carb} to the Fe_{ox} pool and hence any interpretation of ferruginous or euxinic signals would remain robust. The weathering of pyrite to Fe_{ox} would not affect interpretation of anoxic signals ($Fe_{HR}/Fe_T > 0.38$), but may reduce the Fe_{py}/Fe_{HR} ratio, giving a false ferruginous signal in a euxinic sample. In the extreme and highly unlikely scenario that all Fe_{ox} in our samples is a product of pyrite weathering, ~10% of the anoxic samples would give a euxinic signal. However, significant Fe_{carb} (>20% of the Fe_{HR} fraction) occurs in ~57% of anoxic samples, indicating that the rocks have not been completely weathered and hence this extreme scenario is unlikely.

Data availability. All relevant data are available to download in the data repository associated with this manuscript and further details on the Fe-speciation data are available in ref. 5.

References

1. Poulton, S. W. & Canfield, D. E. Ferruginous conditions: a dominant feature of the ocean through earth's history. *Elements* **7,** 107–112 (2011).
2. Johnston, D. T. *et al.* Late Ediacaran redox stability and metazoan evolution. *Earth Planet. Sci. Lett.* **335,** 25–35 (2012).
3. Planavsky, N. J. *et al.* Low Mid-Proterozoic atmospheric oxygen levels and the delayed rise of animals. *Science* **346,** 635–638 (2014).
4. Canfield, D. E., Poulton, S. W. & Narbonne, G. M. Late-Neoproterozoic deep-ocean oxygenation and the rise of animal life. *Science* **315,** 92–95 (2007).
5. Wood, R. A. *et al.* Dynamic redox conditions control late Ediacaran ecosystems in the Nama Group, Namibia. *Precambrian Res.* **261,** 252–271 (2015).
6. Scott, C. *et al.* Tracing the stepwise oxygenation of the Proterozoic ocean. *Nature* **452,** 456–459 (2008).
7. Chen, X. *et al.* Rise to modern levels of ocean oxygenation coincided with the Cambrian radiation of animals. *Nat. Commun.* **6,** 7142 (2015).
8. Poulton, S. W., Fralick, P. W. & Canfield, D. E. Spatial variability in oceanic redox structure 1.8 billion years ago. *Nat. Geosci.* **3,** 486–490 (2010).
9. Guilbaud, R., Poulton, S. W., Butterfield, N. J., Zhu, M. & Shields-Zhou, G. A. A global transition to ferruginous conditions in the early Neoproterozoic oceans. *Nat. Geosci.* **8,** 466–470 (2015).
10. Sperling, E. A. *et al.* Statistical analysis of iron geochemical data suggests limited late Proterozoic oxygenation. *Nature* **523,** 451–454 (2015).
11. Nursall, J. Oxygen as a prerequisite to the origin of the Metazoa. *Nature* **183,** 1170–1172 (1959).
12. Lenton, T. M., Boyle, R. A., Poulton, S. W., Shields-Zhou, G. A. & Butterfield, N. J. Co-evolution of eukaryotes and ocean oxygenation in the Neoproterozoic era. *Nat. Geosci.* **7.4,** 257–265 (2014).
13. Butterfield, N. J. Oxygen, animals and oceanic ventilation: an alternative view. *Geobiology* **7,** 1–7 (2009).

14. Mills, D. B. *et al.* Oxygen requirements of the earliest animals. *Proc. Natl Acad. Sci. USA* **111,** 4168–4172 (2014).
15. Macdonald, F. A., Pruss, S. B. & Strauss, J. V. Trace fossils with spreiten from the late Ediacaran Nama Group,Namibia: complex feeding patterns five million years before the Precambrian–Cambrian boundary. *J. Paleontol.* **88,** 299–308 (2014).
16. Grotzinger, J. P., Watters, W. A. & Knoll, A. H. Calcified metazoans in thrombolite-stromatolite reefs of the terminal Proterozoic Nama Group, Namibia. *Paleobiology* **26,** 334–359 (2000).
17. Penny, A. *et al.* Ediacaran metazoan reefs from the Nama Group, Namibia. *Science* **344,** 1504–1506 (2014).
18. Wood, R. A., Grotzinger, J. P. & Dickson, J. A. D. Proterozoic modular biomineralized metazoan from the Nama Group, Namibia. *Science* **296,** 2383–2386 (2002).
19. Gibson, R. & Atkinson, R. Oxygen minimum zone benthos: adaptation and community response to hypoxia. *Oceanogr. Marine Biol. Annu. Rev.* **41,** 1–45 (2003).
20. Sperling, E. A. *et al.* Oxygen, facies, and secular controls on the appearance of Cryogenian and Ediacaran body and trace fossils in the Mackenzie Mountains of northwestern Canada. *Geol. Soc. Ame. Bull.* **128.3-4,** 558–575 (2015).
21. Johnson, K. S. *et al.* Manganese flux from continental margin sediments in a transect through the oxygen minimum. *Science* **257,** 1242–1245 (1992).
22. Klinkhammer, G. P. & Bender, M. L. The distribution of manganese in the Pacific Ocean. *Earth Planet. Sci. Lett.* **46,** 361–384 (1980).
23. Sholkovitz, E. R., Landing, W. M. & Lewis, B. L. Ocean particle chemistry: the fractionation of rare earth elements between suspended particles and seawater. *Geochim. Cosmochim. Acta* **58,** 1567–1579 (1994).
24. Ohta, A. & Kawabe, I. REE (III) adsorption onto Mn dioxide (MnO_2) and Fe oxyhydroxide: Ce (III) oxidation by MnO_2. *Geochim. Cosmochim. Acta* **65,** 695–703 (2001).
25. De Carlo, E. H. & Green, W. J. Rare earth elements in the water column of Lake Vanda, McMurdo Dry Valleys, Antarctica. *Geochim. Cosmochim. Acta* **66,** 1323–1333 (2002).
26. De Baar, H. J., German, C. R., Elderfield, H. & van Gaans, P. Rare earth element distributions in anoxic waters of the Cariaco Trench. *Geochim. Cosmochim. Acta* **52,** 1203–1219 (1988).
27. Bau, M., Möller, P. & Dulski, P. Yttrium and lanthanides in eastern Mediterranean seawater and their fractionation during redox-cycling. *Marine Chem.* **56,** 123–131 (1997).
28. Webb, G. E. & Kamber, B. S. Rare earth elements in Holocene reefal microbialites: a new shallow seawater proxy. *Geochim. Cosmochim. Acta* **64,** 1557–1565 (2000).
29. Banner, J. L., Hanson, G. N. & Meyers, W. J. Rare earth element and Nd isotopic variations in regionally extensive dolomites from the Burlington-Keokuk Formation (Mississippian): implications for REE mobility during carbonate diagenesis. *J. Sediment. Res.* **58,** 415–432 (1988).
30. Himmler, T., Bach, W., Bohrmann, G. & Peckmann, J. Rare earth elements in authigenic methane-seep carbonates as tracers for fluid composition during early diagenesis. *Chem. Geol.* **277,** 126–136 (2010).
31. Tostevin, R. *et al.* Effective use of cerium anomalies as a redox proxy in carbonate-dominated marine settings. *Chem. Geol.* **438,** 146–162 (2016).
32. Raiswell, R. & Canfield, D. E. Sources of iron for pyrite formation in marine sediments. *Am. J. Sci.* **298,** 219–245 (1998).
33. Hall, M. *et al.* Stratigraphy, palaeontology and geochemistry of the late Neoproterozoic Aar Member, southwest Namibia: Reflecting environmental controls on Ediacara fossil preservation during the terminal Proterozoic in African Gondwana. *Precambrian Res.* **238,** 214–232 (2013).
34. Morris, S. C., Mattes, B. & Chen, M. The early skeletal organism Cloudina: new occurrences from Oman and possibly China. *Am. J. Sci.* 245–260 (1990).
35. Warren, L. V. *et al.* Corumbella and *in situ* Cloudina in association with thrombolites in the Ediacaran Itapucumi Group, Paraguay. *Terra Nova* **23,** 382–389 (2011).
36. Wood, R. A. Paleoecology of the earliest skeletal metazoan communities: implications for early biomineralization. *Earth Sci. Rev.* **106,** 184–190 (2011).
37. Zhuravlev, A. Y., Wood, R. A. & Penny, A. M. Ediacaran skeletal metazoan interpreted as a lophophorate. *Proc. R. Soc. B* **282,** 1818 (2015).
38. Planavsky, N. *et al.* Rare Earth Element and yttrium compositions of Archean and Paleoproterozoic Fe formations revisited: new perspectives on the significance and mechanisms of deposition. *Geochim. Cosmochim. Acta* **74,** 6387–6405 (2010).
39. Slack, J., Grenne, T., Bekker, A., Rouxel, O. & Lindberg, P. Suboxic deep seawater in the late Paleoproterozoic: evidence from hematitic chert and iron formation related to seafloor-hydrothermal sulfide deposits, central Arizona, USA. *Earth Planet. Sci. Lett.* **255,** 243–256 (2007).
40. Mazumdar, A., Tanaka, K., Takahashi, T. & Kawabe, I. Characteristics of rare earth element abundances in shallow marine continental platform carbonates of Late Neoproterozoic successions from India. *Geochem. J.* **37,** 277–289 (2003).
41. Ling, H.-F. *et al.* Cerium anomaly variations in Ediacaran–earliest Cambrian carbonates from the Yangtze Gorges area, South China: implications for oxygenation of coeval shallow seawater. *Precambrian Res.* **225,** 110–127 (2013).
42. German, C. R. & Elderfield, H. Rare earth elements in the NW Indian Ocean. *Geochim. Cosmochim. Acta* **54,** 1929–1940 (1990).
43. Clement, B. G., Luther, III G. W. & Tebo, B. M. Rapid, oxygen-dependent microbial Mn(II) oxidation kinetics at sub-micromolar oxygen concentrations in the Black Sea suboxic zone. *Geochim. Cosmochim. Acta* **73,** 1878–1889 (2009).
44. Saager, P. M., De Baar, H. J. W. & Burkill, P. H. Manganese and iron in Indian Ocean waters. *Geochim. Cosmochim. Acta* **53,** 2259–2267 (1989).
45. Trefry, J. H., Presley, B. J., Keeney-Kennicutt, W. L. & Trocine, R. P. Distribution and chemistry of manganese, iron, and suspended particulates in Orca Basin. *Geo Marine Lett.* **4,** 125–130 (1984).
46. Raiswell, R. & Anderson, T. F. Reactive iron enrichment in sediments deposited beneath euxinic bottom waters: constraints on supply by shelf recycling. *Geol. Soc. Lond. Special Publications* **248,** 179–194 (2005).
47. Levin, L. A., Gage, J. D., Martin, C. & Lamont, P. A. Macrobenthic community structure within and beneath the oxygen minimum zone, NW Arabian Sea. *Deep Sea Res.* **47,** 189–226 (2000).
48. Savrda, C. E. & Bottjer, D. J. Oxygen-related biofacies in marine strata: an overview and update. *Geol. Soc. Lond. Special Publications* **58,** 201–219 (1991).
49. Love, G. D. *et al.* Fossil steroids record the appearance of Demospongiae during the Cryogenian period. *Nature* **457,** 718–721 (2009).
50. Zhang, S. *et al.* Sufficient oxygen for animal respiration 1,400 million years ago. *Proc. Natl Acad. Sci. USA* **113,** 1731–1736 (2016).
51. Knoll, A. H. Biomineralization and Evolutionary History. *Rev. Mineral. Geochem.* **54,** 329–356 (2003).
52. Saylor, B. Z., Kaufman, A. J., Grotzinger, J. P. & Urban, F. A composite reference section for terminal proterozoic strata of Southern Namibia. *SEPM J. Sediment. Res.* **68,** 1223–1235 (1998).
53. Saylor, B. Z., Grotzinger, J. P. & Germs, G. J. B. Sequence stratigraphy and sedimentology of the Neoproterozoic Kuibis and Schwarzrand Subgroups (Nama Group), southwestern Namibia. *Precambrian Res.* **73,** 153–171 (1995).
54. Grotzinger, J. P., Bowring, S. A., Saylor, B. Z. & Kaufman, A. J. Biostratigraphic and geochronologic constraints on early animal evolution. *Science* **270,** 598–604 (1995).
55. Grotzinger, J. & Miller, R. *The Nama Group* 2 Geological Society of Namibia, 2008).
56. Narbonne, G. *et al.* The Ediacaran Period. *Geol. Time Scale* 413–435 (2012).
57. Germs, G. J. B. Implications of a sedimentary facies and depositional environmental analysis of the Nama group in South West Africa/Namibia. *Geol. Soc. South Africa* **11,** 89–114 (1983).
58. Narbonne, G. M., Saylor, B. Z. & Grotzinger, J. P. The youngest Ediacaran fossils from southern Africa. *J. Paleontol.* **71.06,** 953–967 (1997).
59. Bau, M. & Dulski, P. Distribution of yttrium and rare-earth elements in the Penge and Kuruman iron-formations, Transvaal Supergroup, South Africa. *Precambrian Res.* **79,** 37–55 (1996).
60. Sunda, W. G. & Huntsman, S. A. Effect of sunlight on redox cycles of manganese in the southwestern Sargasso Sea. *Deep Sea Res. A Oceanogr. Res. Papers* **35,** 1297–1317 (1988).
61. Bau, M., Koschinsky, A., Dulski, P. & Hein, J. R. Comparison of the partitioning behaviours of yttrium, rare earth elements, and titanium between hydrogenetic marine ferromanganese crusts and seawater. *Geochim. Cosmochim. Acta* **60,** 1709–1725 (1996).
62. German, C. R. & Elderfield, H. Application of the Ce anomaly as a paleoredox indicator: The ground rules. *Paleoceanography* **5,** 823–833 (1990).
63. Shields, G. & Webb, G. Has the REE composition of seawater changed over geological time? *Chem. Geol.* **204.1,** 103–107 (2004).
64. Pourmand, A., Dauphas, N. & Ireland, T. J. A novel extraction chromatography and MC-ICP-MS technique for rapid analysis of REE, Sc and Y: revising CI-chondrite and Post-Archean Australian Shale (PAAS) abundances. *Chem. Geol.* **291,** 38–54 (2012).
65. Bau, M. *et al.* Discriminating between different genetic types of marine ferro-manganese crusts and nodules based on rare earth elements and yttrium. *Chem. Geol.* **381,** 1–9 (2014).
66. Haley, B. A., Klinkhammer, G. P. & McManus, J. Rare earth elements in pore waters of marine sediments. *Geochim. Cosmochim. Acta* **68,** 1265–1279 (2004).
67. Poulton, S. W. & Canfield, D. E. Development of a sequential extraction procedure for iron: implications for iron partitioning in continentally derived particulates. *Chem. Geol.* **214,** 209–221 (2005).
68. Canfield, D. E., Raiswell, R., Westrich, J. T., Reaves, C. M. & Berner, R. A. The use of chromium reduction in the analysis of reduced inorganic sulfur in sediments and shales. *Chem. Geol.* **54,** 149–155 (1986).

69. Clarkson, M. O., Poulton, S. W., Guilbaud, R. & Wood, R. A. Assessing the utility of Fe/Al and Fe-speciation to record water column redox conditions in carbonate-rich sediments. *Chem. Geol.* **382,** 111–122 (2014).
70. Turekian, K. K. & Wedepohl, K. H. Distribution of the Elements in Some Major Units of the Earth's Crust. *Geol. Soc. Am. Bull.* **72,** 175–192 (1961).

Acknowledgements

R.T., R.A.W., G.A.S.Z., S.W.P., R.G., F.B. and A.R.P. acknowledge financial support from NERC's Co-evolution of Life and the Planet scheme (NE/1005978/1). Support was provided to M.O.C. and A.R.P. through the International Centre for Carbonate Reservoirs (ICCR). F.B. acknowledges support from the Laidlaw Hall fund. We are grateful for access to farms and thank A. Horn of Omkyk, U. Schulze Neuhoff of Ababis, L. and G. Fourie of Zebra River, C. Husselman of Driedornvlagte and L.G. Evereet of Arasab and Swartpunt. We thank Gary Tarbuck and Jim Davy for technical support, and Gerd Winterleitner and Tony Prave for help carrying out field work.

Author contributions

R.A.W., K.H.H., R.T., A.M.P., F.B. and A.C. collected the samples. M.O.C., R.T., A.M.P. and F.B. prepared the samples. R.T. conceived the project and analysed the samples. R.T. interpreted the Ce anomaly data, after discussions with G.A.S., T.H., R.G. and S.W.P. R.T. wrote the paper with S.W.P., G.A.S., R.A.W., and R.G. and input from all co-authors.

Additional information

Supplementary Information accompanies this paper at http://www.nature.com/naturecommunications

Competing financial interests: The authors declare no competing financial interest.

Reprints and permission information is available online at http://npg.nature.com/reprintsandpermissions/

How to cite this article: Tostevin, R. *et al.* Low-oxygen waters limited habitable space for early animals. *Nat. Commun.* 7:12818 doi: 10.1038/ncomms12818 (2016).

Supplementary Figures

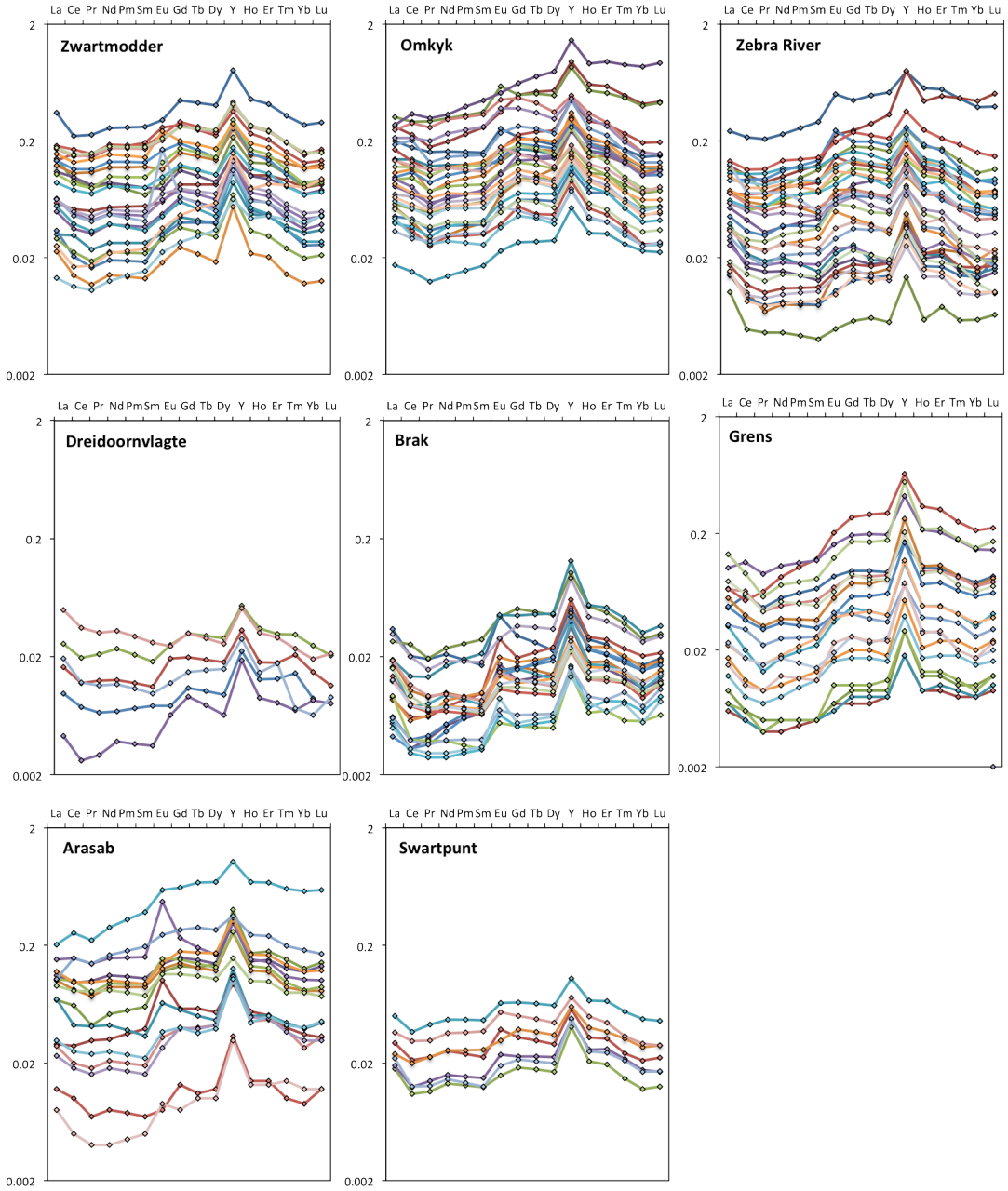

Supplementary Figure 1: REY spider diagrams for each locality, screened for samples with Y/Ho>67.

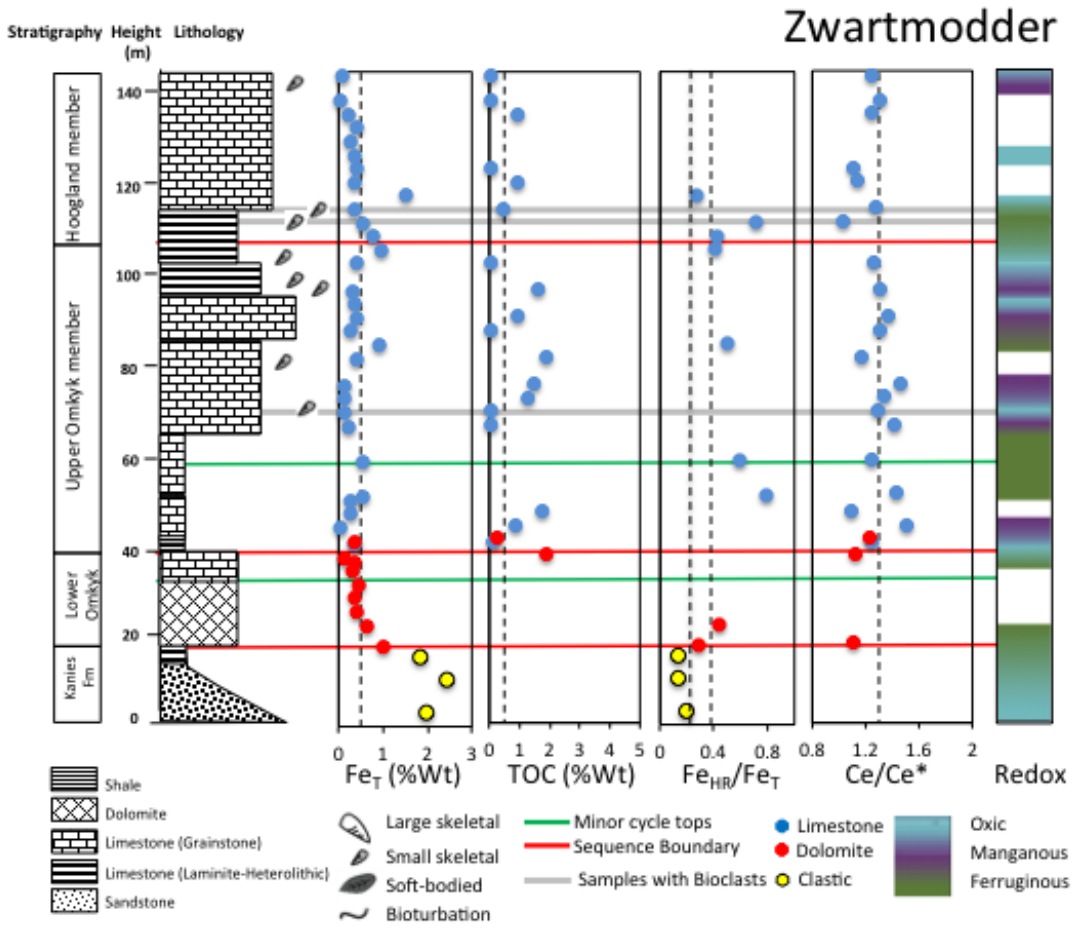

Supplementary Figure 2: Stratigraphic and data summary for Zwartmodder

Fe_T, Fe_{HR}/Fe_T, TOC[2] and Ce_{SN}/Ce^*_{SN} data for inner ramp Zwartmodder from the Kuibis Subgroup in the Zaris Basin, alongside stratigraphic log[2]. The final column represents our best interpretation of redox based on all these data.

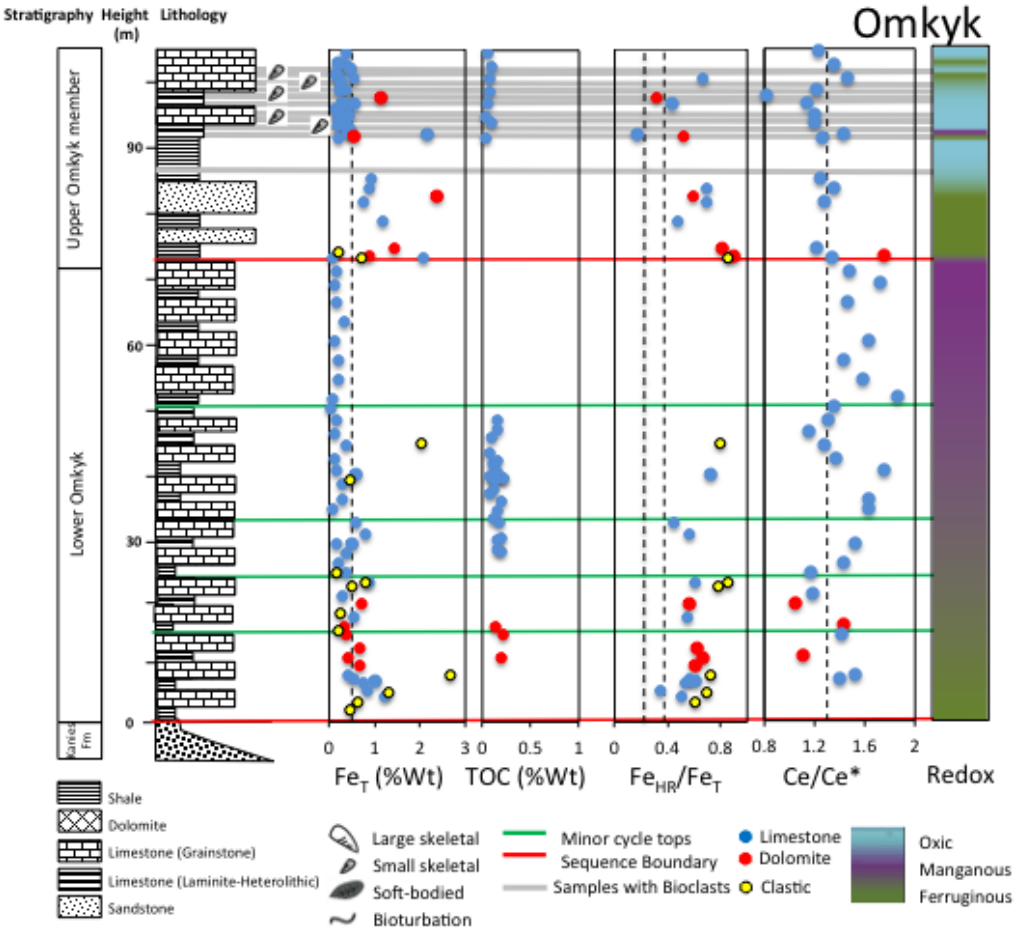

Supplementary Figure 3: Stratigraphic and data summary for Omkyk

Fe_T, Fe_{HR}/Fe_T, TOC[2] and Ce_{SN}/Ce^*_{SN} data for deep inner ramp Omkyk from the Kuibis Subgroup in the Zaris Basin, alongside stratigraphic log[2]. The final column represents our best interpretation of redox based on all these data.

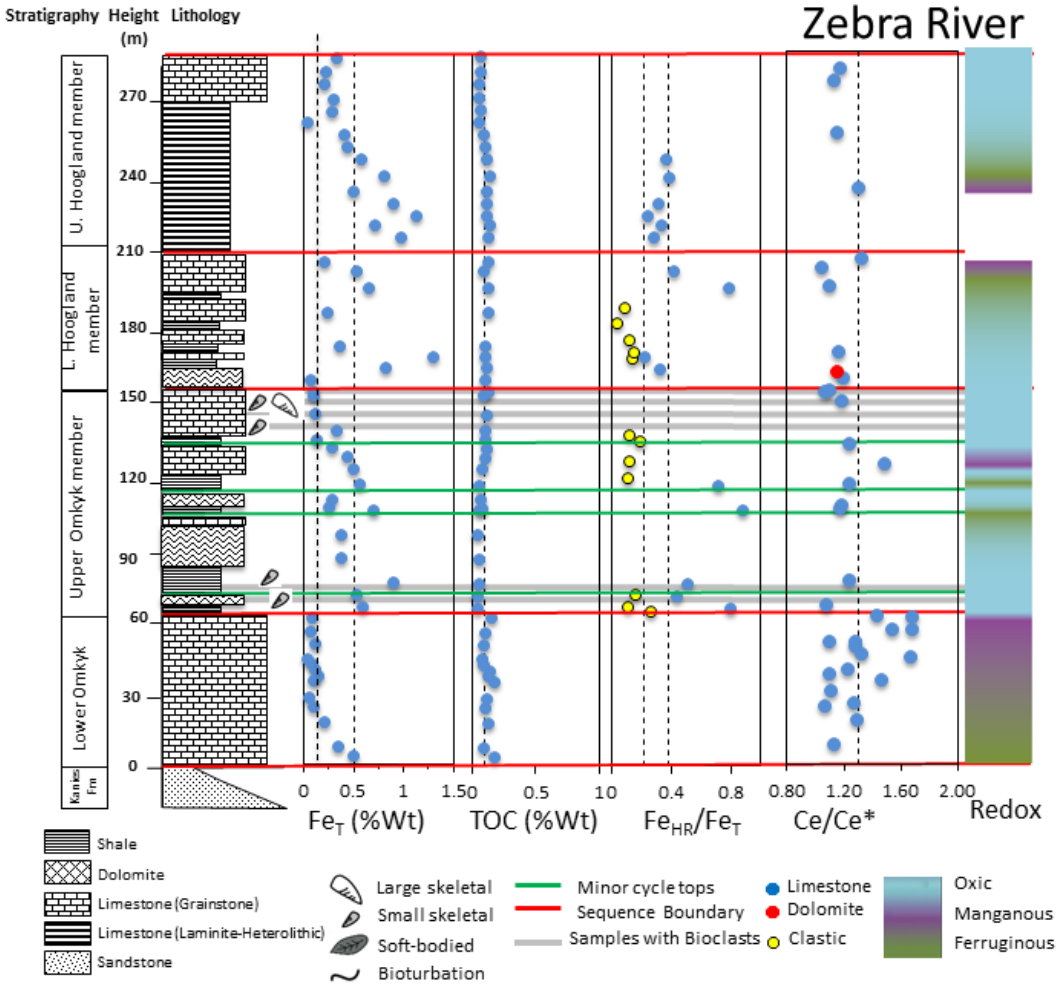

Supplementary Figure 4: Stratigraphic and data summary for Zebra River

Fe_T, Fe_{HR}/Fe_T, TOC[2] and Ce_{SN}/Ce^*_{SN} data for deep inner ramp Zebra River from the Kuibis Subgroup in the Zaris Basin, alongside stratigraphic log[2]. The final column represents our best interpretation of redox based on all these data.

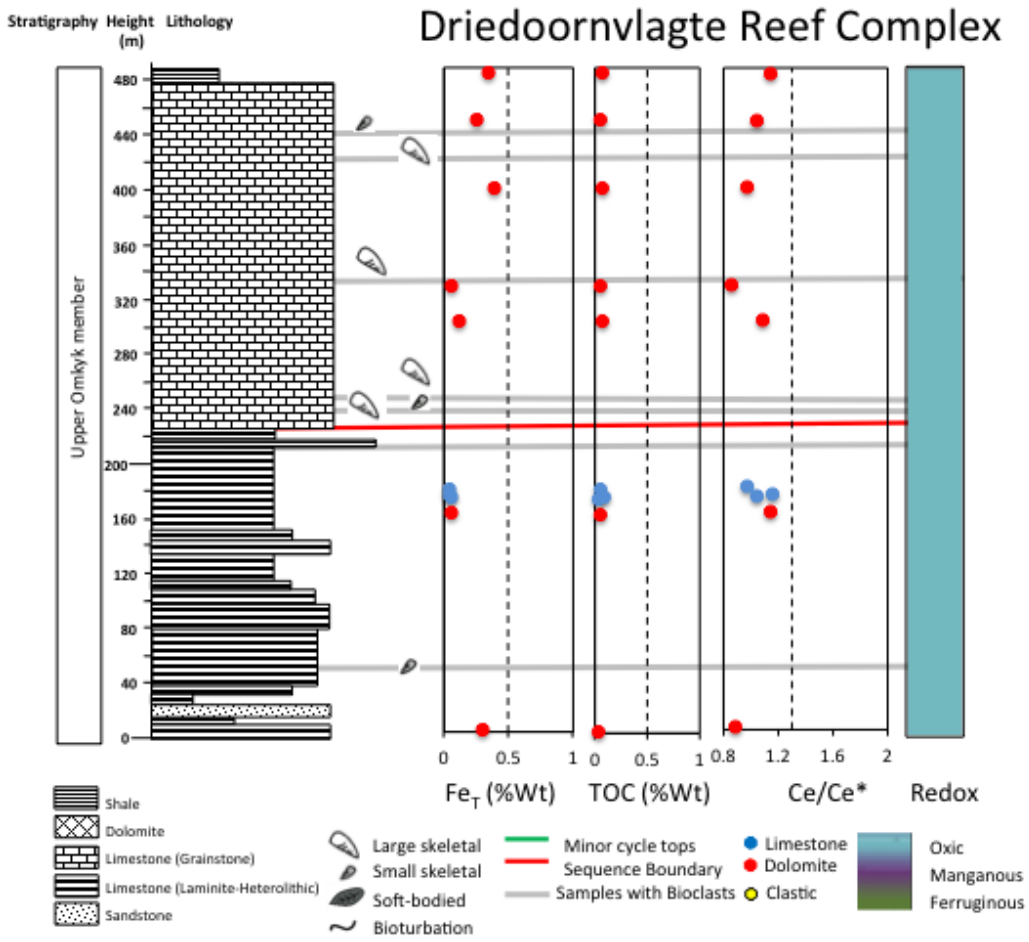

Supplementary Figure 5: Stratigraphic and data summary for Dreidoornvlagte

Fe_T, Fe_{HR}/Fe_T, TOC[2] and Ce_{SN}/Ce^*_{SN} data for mid-ramp pinnacle reef Driedoornvlagte from the Kuibis Subgroup in the Zaris Basin, alongside stratigraphic log.[2] The final column represents our best interpretation of redox based on all these data.

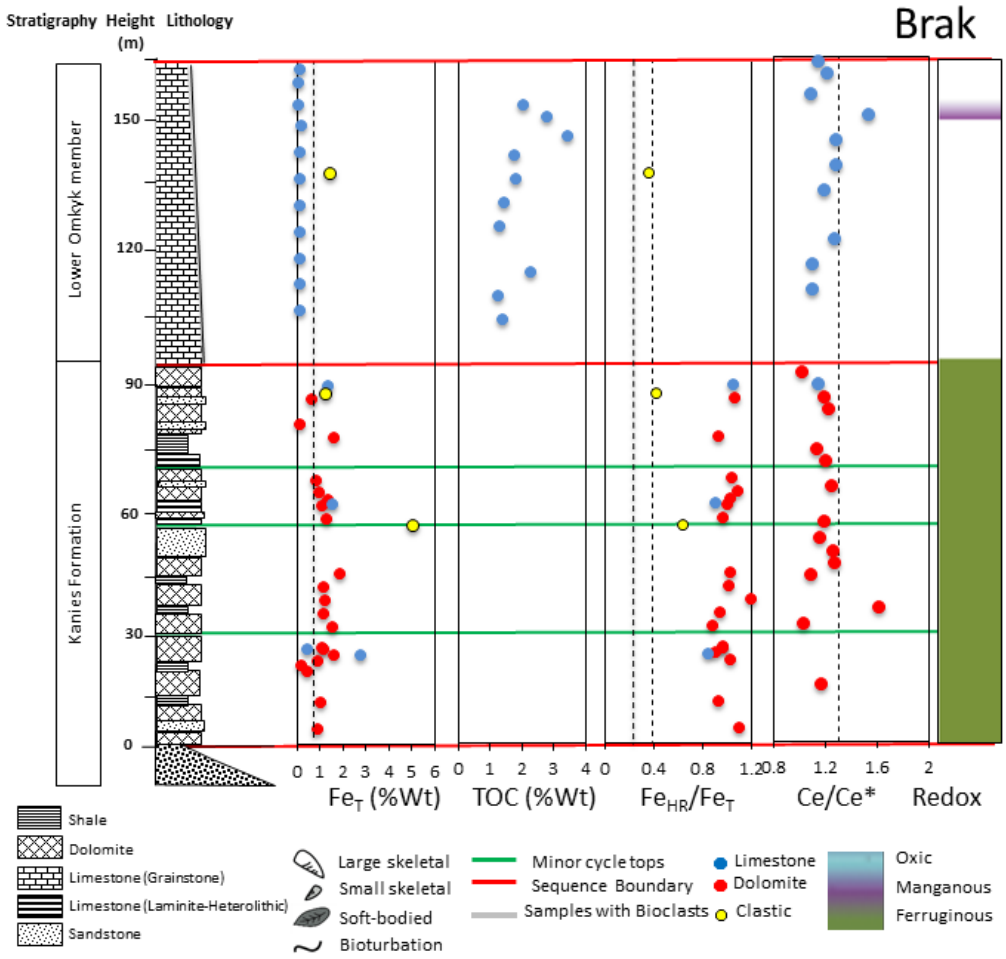

Supplementary Figure 6: Stratigraphic and data summary for Brak

Fe_T, Fe_{HR}/Fe_T, TOC[2] and Ce_{SN}/Ce^*_{SN} data for outer ramp Brak from the Kuibis Subgroup in the Zaris Basin, alongside stratigraphic log[2]. The final column represents our best interpretation of redox based on all these data.

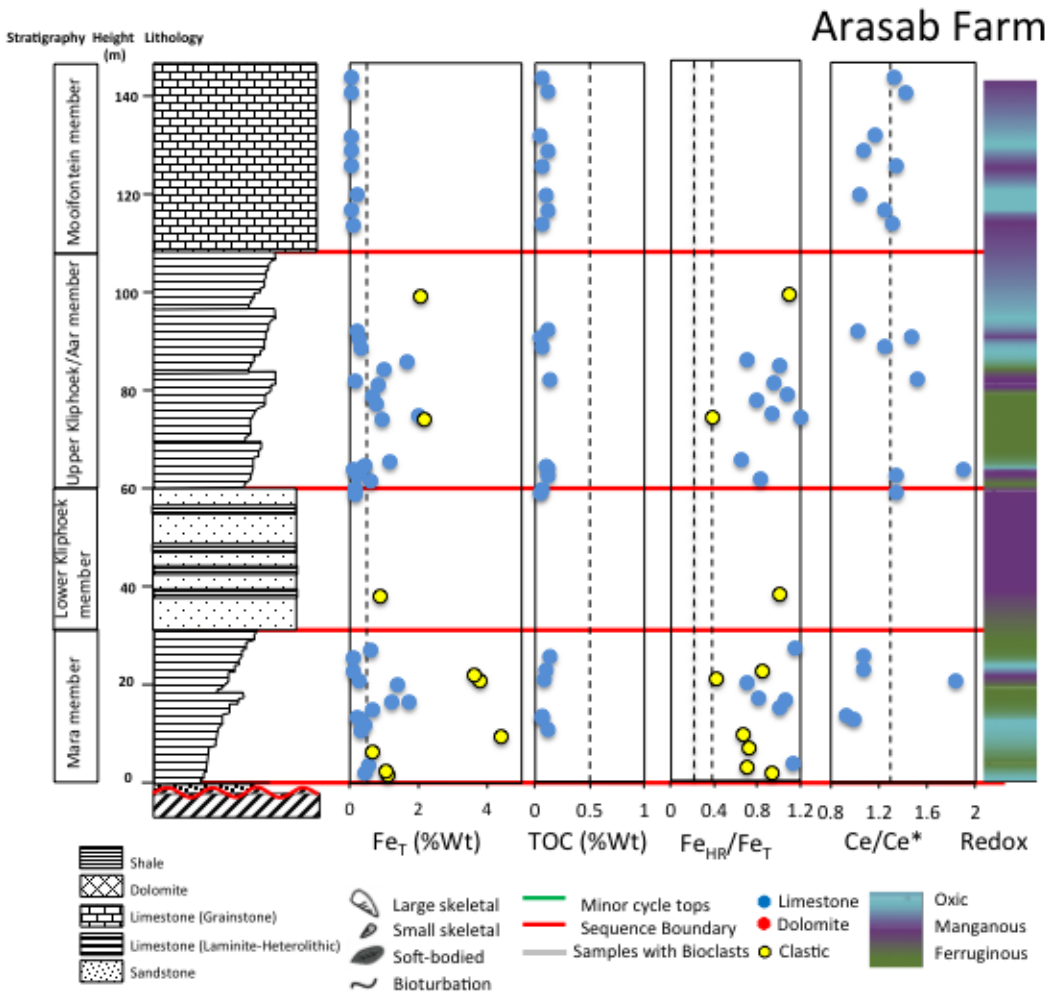

Supplementary Figure 7: Stratigraphic and data summary for Arasab

Fe_T, Fe_{HR}/Fe_T, TOC[2] and Ce_{SN}/Ce^*_{SN} data for inner ramp Arasab from the Kuibis Subgroup in the Witputs Basin, alongside stratigraphic log[2]. The final column represents our best interpretation of redox based on all these data.

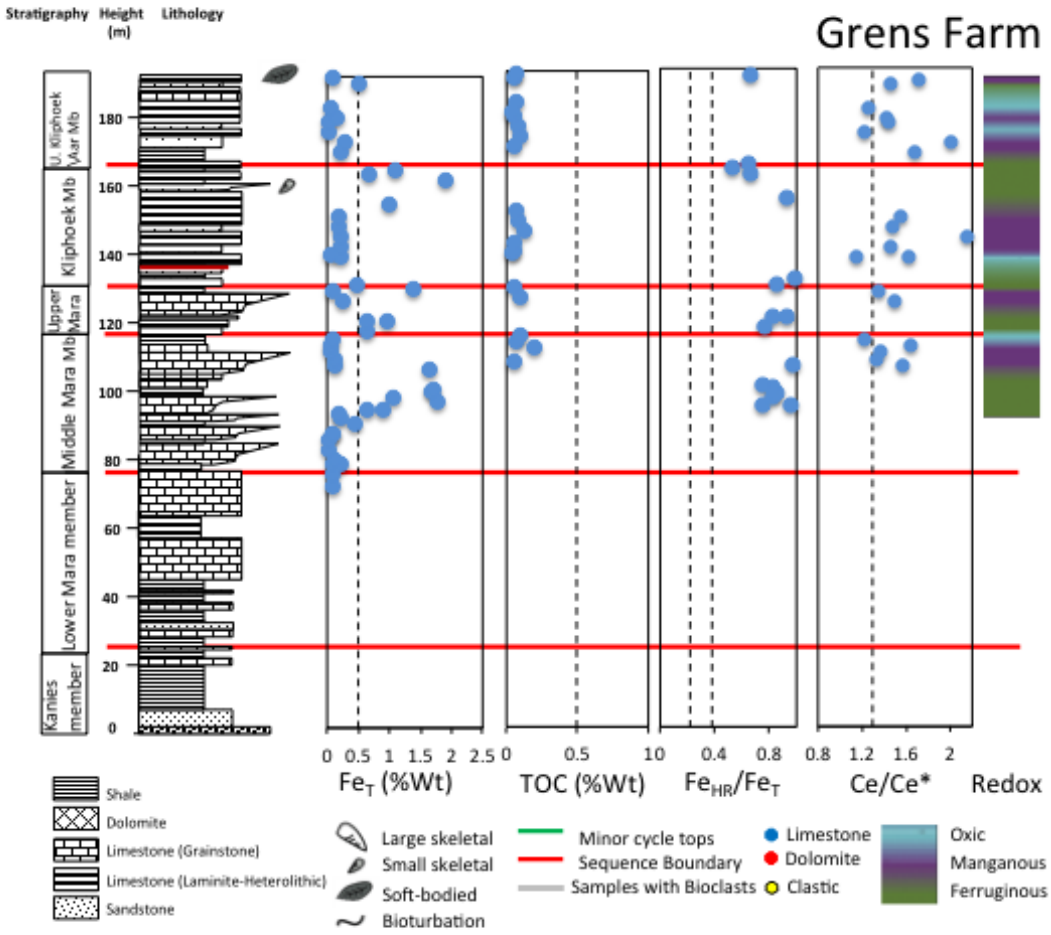

Supplementary Figure 8: Stratigraphic and data summary for Grens

Fe_T, Fe_{HR}/Fe_T, TOC and Ce_{SN}/Ce^*_{SN} data for inner ramp Grens from the Kuibis Subgroup in the Witputs Basin, alongside stratigraphic log[2]. The final column represents our best interpretation of redox based on all these data.

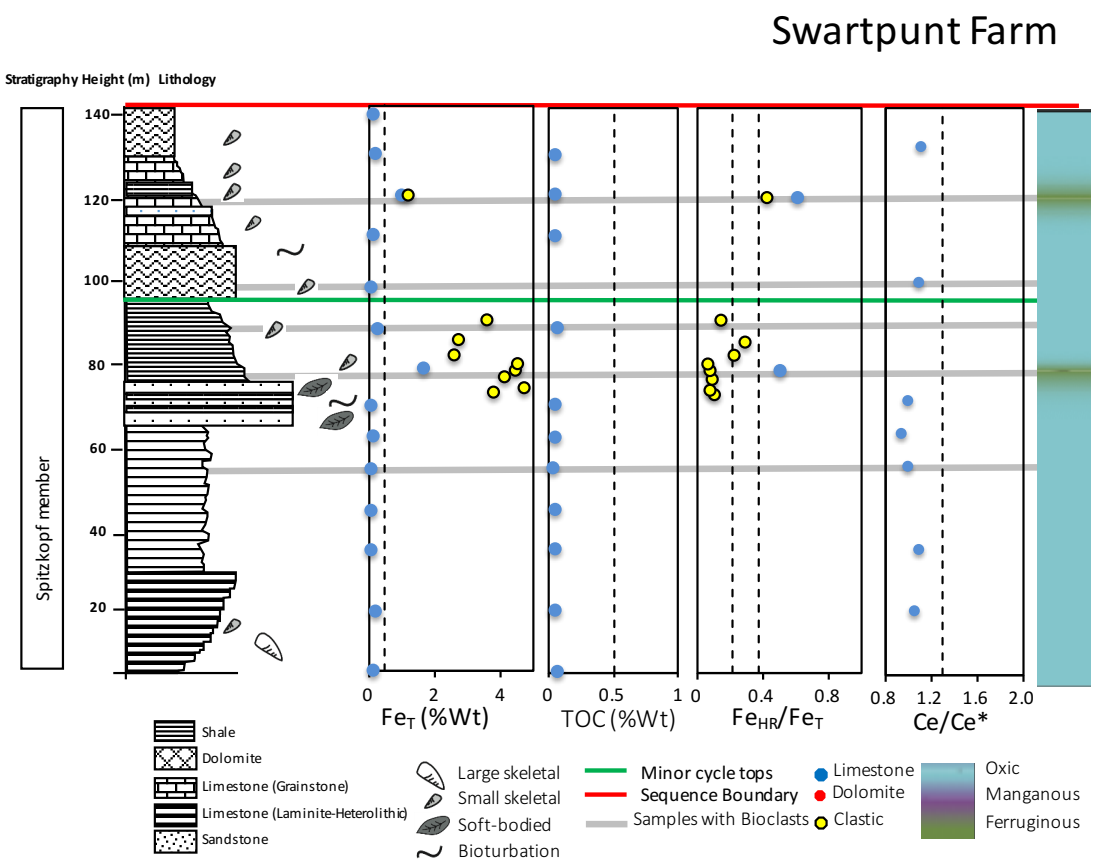

Supplementary Figure 9: Stratigraphic and data summary for Swartpunt

Fe_T, Fe_{HR}/Fe_T, TOC[2] and Ce_{SN}/Ce^*_{SN} data for inner ramp Swartpunt from the Schwarzrand Subgroup in the Witputs Basin, alongside stratigraphic log[2]. The final column represents our best interpretation of redox based on all these data.

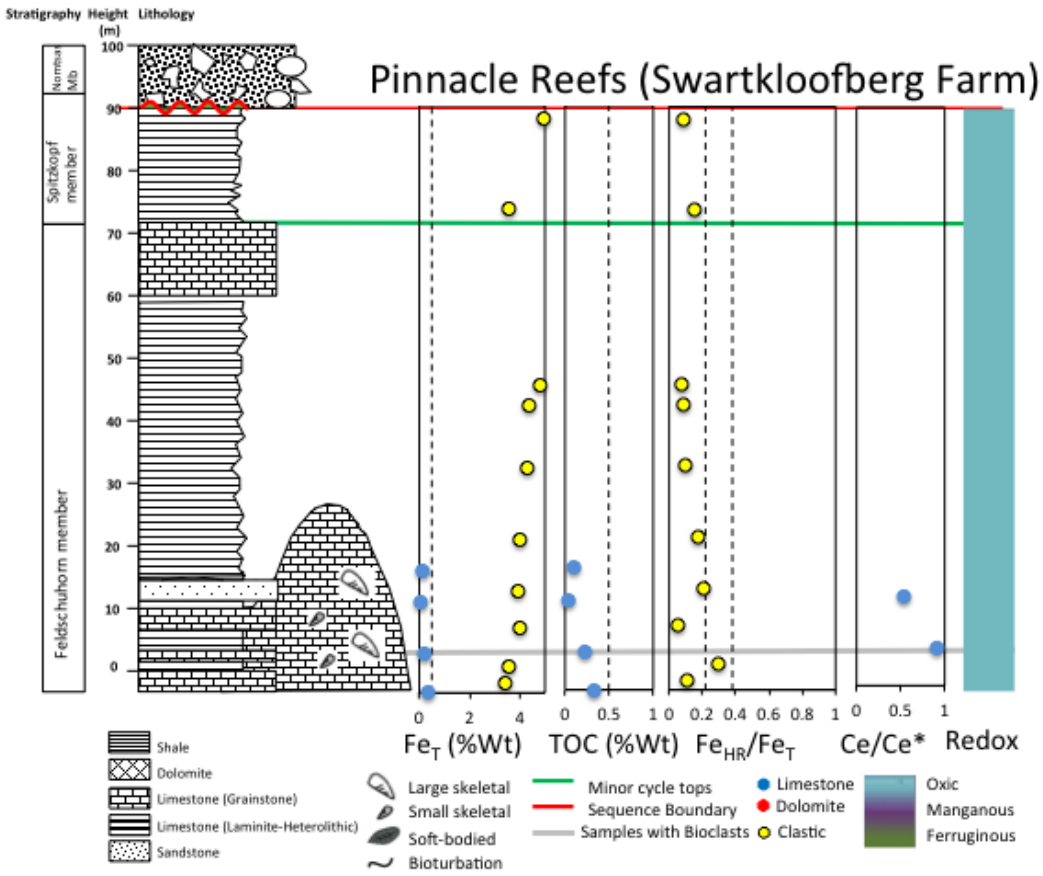

Supplementary Figure 10: Stratigraphic and data summary for the Pinnacle Reefs

Fe_T, Fe_{HR}/Fe_T, TOC[2] and Ce_{SN}/Ce^*_{SN} data for inner ramp Pinnacle reef from the Schwarzrand Subgroup in the Witputs Basin, alongside stratigraphic log[2]. The final column represents our best interpretation of redox based on all these data.

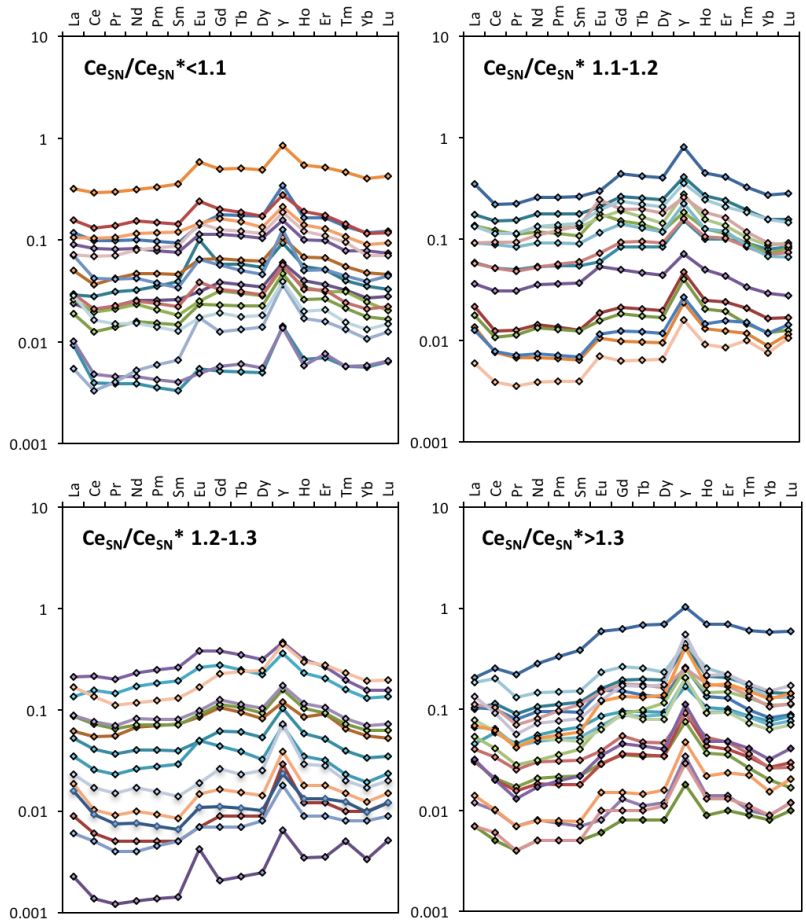

Supplementary Figure 11: **Comparison of REY spider diagrams for examples with no Ce anomaly (<1.3), and those with a positive Ce anomaly (>1.3).**

Both show seawater features, including positive Y and La anomalies, and some samples show small positive Eu anomalies. REY patterns for samples with no positive Ce anomaly are divided into categories <1.1, 1.1-1.2 and 1.2—1.3, to demonstrate the utility of 1.3 as an appropriate cut off for genuine Ce enrichments above background fluctuations.

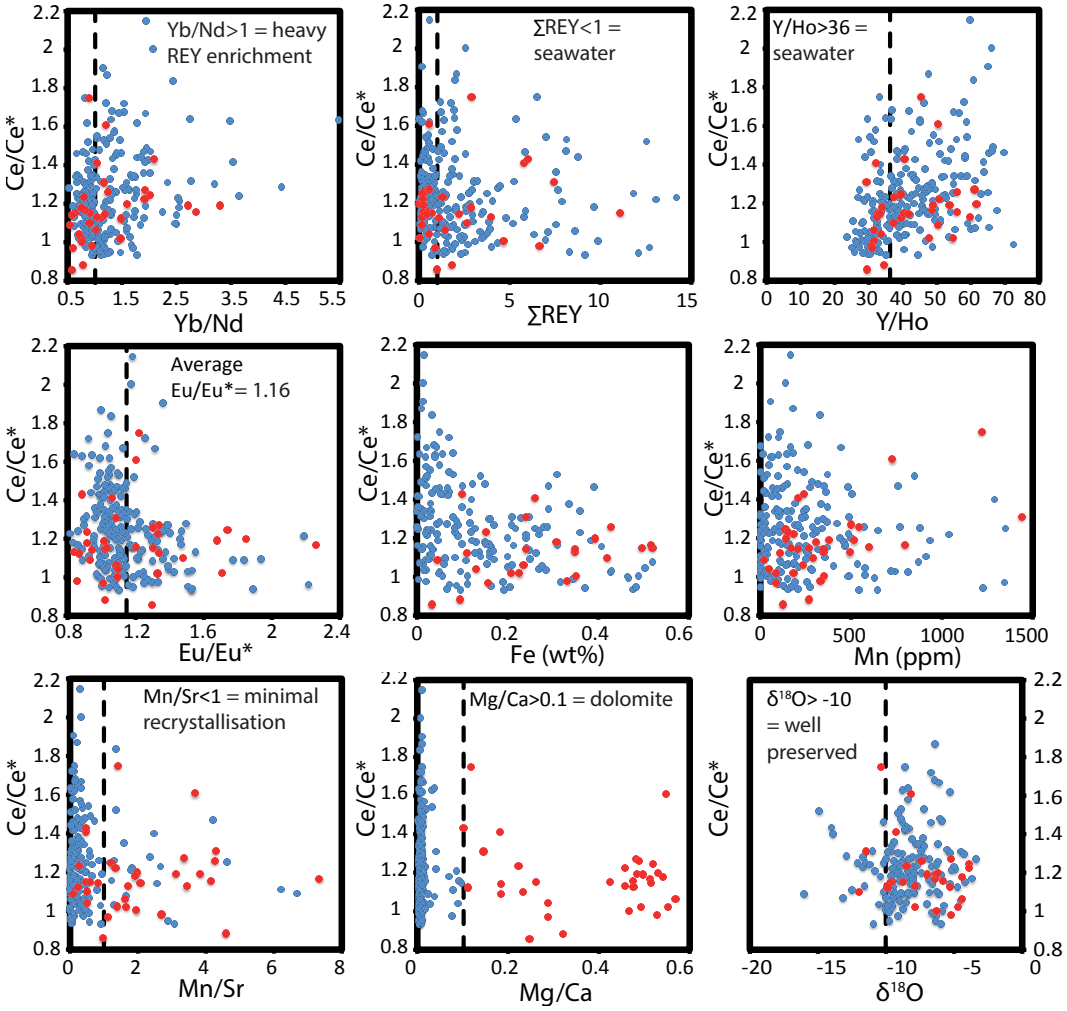

Supplementary Figure 12: Positive Ce anomalies against common REY, major element and isotopic parameters for assessing data quality.

Key threshold values highlighted by dashed lines. Red = dolomite, blue = limestone.

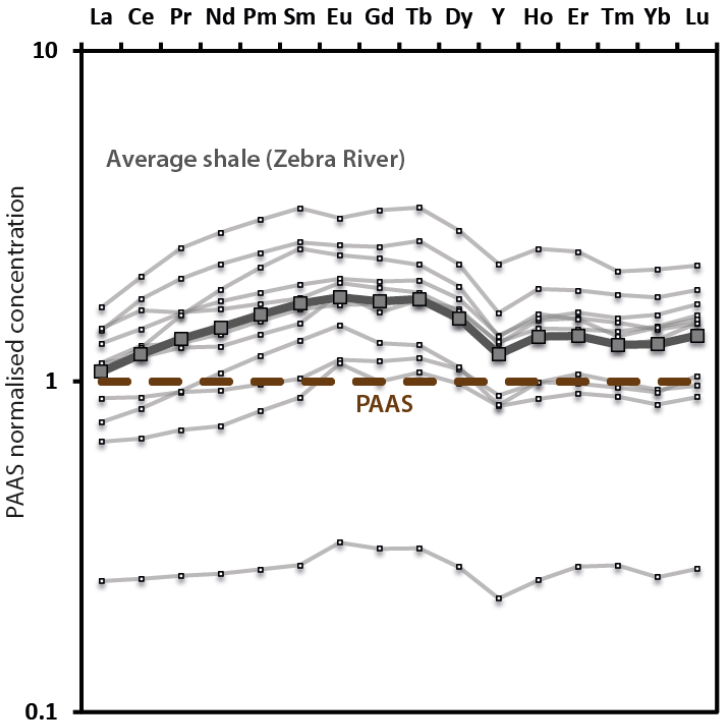

Supplementary Figure 13: Rare earth elements for shales from Zebra River section.

Data are normalised to PAAS, and show small negative Y anomalies and minor MREE enrichment, but no anomalous Ce behaviour. Thick grey line represent average shale values for Zebra River, and brown dashed line represents international shale standard, PAAS[1].

Supplementary Tables

Supplementary Table 1. Co-ordinates and names and Site numbers for all sampled sections.

Relative water depths are indicated, assessed based on sedimentology[2]

Section	Longitude	Latitude	Relative water depth
Site 1: Zwartmodder	16°19'31.00"E	24°53'41.00"S	Shallow inner ramp
Site 2: Omkyk	16°13'45.00"E	24°48'19.00"S	Deep inner ramp
Site 3: Zebra River	16°12'13.24" E	24°30' 49.38"S	Deep inner ramp
Site 4: Driedornvlagte	16°39' 50.57"E	23°51' 36.83"S	Mid ramp
Site 5: Brak	16°8'6.50"E	23°58'17.00"S	Outer ramp
Site 6: Arasab	16°24'47.00"E	26°53'15.00"S	Shallow inner ramp
Site 7: Grens	16°21'58.50"E	27°10'34.50"S	Shallow inner ramp
Site 8: Pinnacle Reefs	16°3’40.60"E	27°27’52.70"S	Mid ramp
Site 9: Swartpunt	16°41'33.00"E	27°28'29.00"S	Shallow inner ramp

Supplementary Notes

Supplementary Note 1 - Sequence Stratigraphy

The Zaris and Witputs Basins have distinct stratigraphic frameworks[3,4], but common features such as systems tracts and sequence boundaries can be correlated across the Osis Arch, which separates the two sub-basins[5,6]. The basal unit in both basins is the siliciclastic Kanies Member. In the Zaris Basin, this is overlain by thick carbonate dominated units of the Omkyk and Hoogland Members. The Omkyk member is typified by decimeter-scale, upwards coarsening, mid-inner to shoreface cycles. The overlying Hoogland Member is a deeper water mid-inner ramp to middle shoreface settings, recording transgressive-regressive depositional cycles in heterolithic interbeds. In the Witputs Basin, the Kanies Member is overlain by the carbonate dominated Mara Member deposited during a highstand systems tract. The Mara Member is overlain by the transgressive systems tract of the Kliphoek Member, typified by upper shoreface to tide-dominated shoreline sandstones[3]. The overlying Mooifontein Member is a thin-bedded shallow-marine limestone, the top of which is marked by a conglomerate-filled unconformity with canyon-like erosional relief[4].

The younger Schwarzrand Group, sampled in the Witputs Basin, records mostly shallow marine mixed clastic and carbonate rocks in the lower Urusis Formation. The middle part consists of carbonate dominated Huns, Feldschuhorn and Spitzkopf Member, including pinnacle reefs that initiate on the flooding surface at the top of the Huns Member and are enveloped by the overlying shales of the

Feldschuhorn Member. The top of the Schwarzrand Group is the conglomeratic Nomstas Formation, that infills incised valleys, bracketed by ash beds dated at 542.68 ± 1.245 Ma and 540.61 ± 0.67 Ma (U–Pb zircon)[7].

Typical late Ediacaran fossils, such as *Ernietta, Pteridinium, Swartpuntia,* and *Rangea*[8], vendotaenids[9], and Ediacaran skeletal fossils, *Cloudina*[5,10], *Namacalathus*[11] and *Namapoikia*[12], have been described from both the Zaris and Witputs Basins[2]. The oldest reported *Cloudina* is from the carbonate-dominated Mara Member in the Witputs Basin[5]. The oldest Ediacara-type fossils occur in the Mara Member of the Kuibis Subgroup in the Witputs Basin[3], and the youngest, including *Swartpuntia*, are found 60 m below the Ediacaran–Cambrian unconformity in the more southerly portion of the Witputs Basin[8].

Supplementary Note 2 – Section and data descriptions

Zwartmodder was deposited predominantly in shallow, proximal ramp settings. The section is dominated by dolomites at the base, shallowing to mainly limestone laminates, packstones and grainstones towards the top of the section. There are horizons of abundant skeletal animals in the Upper Omkyk Member highstand systems tract (HST) and Lower Hoogland Member transgressive systems tract (TST), and minor thrombolites in the Upper Omkyk Member HST[2]. There is at least one horizon with large skeletal fossils. Zwartmodder shows fluctuating anoxia, with Fe_{HR}/Fe_T >0.38 interbedded with carbonates with low Fe_T[2]. Other samples with low Fe_T have high TOC, giving an equivocal signal. Both Fe_T and TOC are variable, from 0 to ~2 wt% and 0.04 to 5.66wt%, respectively

(Supplementary Fig 5). Intervals where Fe_T is <0.5 wt% are intermittent in the Upper Omkyk Member TST and HST, and Lower Hoogland Member TST, and are interpreted to represent probable oxic horizons. Fe speciation in shales in the Kanies at the base of the section indicates an oxic signature. Limited carbonate samples with FeT > 0.5 wt% indicate intermittently anoxic ferruginous conditions in the Lower Omkyk Member TST and Upper Omkyk Member TST and HST, and Lower Hoogland Member TST. Positive Ce anomalies are prevalent but do not reach values as high as in deeper inner-ramp sections [range: 1.04–1.51, average: 1.26±0.13 (1 s.d.)] (Supplementary Fig 5). Across all samples the average Y anomaly =75.0, BSI =1.2, Eu/Eu* =1.1 Yb_{SN}/Nd_{SN} =1.1, and ∑REE =2.68 ppm.

At deep inner-ramp Omkyk, the lower part of the succession is dominated by slope turbidites, slumps and storm-beds and then shallows in the upper part to limestone grainstones showing tidal influence, together with limited thrombolites and abundant skeletal animals. Some shoaling cycles contain evidence for deposition in supra- to inter-tidal conditions, which may have been subjected to exposure and evaporitic conditions. There are horizons of abundant skeletal animals in the Upper Omkyk Member late TST only[2]. Omkyk shows very similar stratigraphic patterns to Zebra River (Supplementary Fig 7), with some stable periods of oxygenated conditions towards the top of both the Lower and Upper Omkyk Member. Fe_T is highly variable, from 0.02 to 2.66 wt%. (Supplementary Fig 6). Carbonate intervals where Fe_T is <0.5 wt% are intermittent in the Lower and Upper Omkyk Member TST and HST, and are interpreted to represent probable oxic horizons. Fe speciation in carbonates and

shales throughout the lower part of the Lower Omkyk Member, and the Upper Omkyk Member indicates anoxic ferruginous conditions. Positive Ce anomalies increase up to the top of the Lower Omkyk Member [range: 1.04-1.87, average: 1.39±0.22 (1 s.d.)], suggesting these conditions were manganous, rather than well-oxygenated. In the Upper Omkyk Member, Ce anomalies are close to 1 [range: 0.83-1.75, average: 1.28±0.20 (1 s.d.)]. There is one carbonate sample, containing biota, that is identified as 'oxic' via Fe-speciation (Fe_{HR}/Fe_T <0.22) [Ref 2], and is associated with a positive Ce anomaly, indicating manganous low oxygen conditions. Another sample containing biota is associated with a negative Ce anomaly indicating well-oxygenated conditions. One sample containing skeletal biota is associated with an anoxic ferruginous signal (Fe_{HR}/Fe_T >0.38), but the remaining biota-bearing samples are associated with low Fe_T and an equivocal Ce_{SN}/Ce^*_{SN} close to 1. Across all samples the average Y anomaly =68.4, BSI =1.2, Eu/Eu* =1.1 Yb_{SN}/Nd_{SN} =1.3, and ∑REE =5.5 ppm.

At the deep inner-ramp locality, Zebra River, the Lower Omkyk Member is dominated by grainstones. In the TST of the Upper Omkyk Member, thrombolite-stromatolite reefs nucleate, forming laterally continuous biostrome layers. *Cloudina* and *Namacalathus* can be found within thrombolite heads and lag beds within inter-reef shales. Towards the top of the Upper Omkyk Member the section shallows into grainstone dominated facies with subordinate shale horizons, containing thinner, discontinuous biostrome microbial reef systems, and some large Namacalathus <35 mm^2. Trace fossils are reported from sandstone lenses at nearby Donkergange Farm[13]. The Hoogland Member contains storm dominated laminites and heterolithics, shallowing towards

grainstone-dominated facies. At Zebra River, Fe-speciation identifies persistent oxygenation, with anoxic ferruginous conditions confined to short-lived horizons[2] (Supplementary Fig 7). Fe_T in carbonate rocks is highly variable, from 0.03 to 1.28 wt%, and follows sequence stratigraphic changes with elevated Fe_T at the base of sequences during early TSTs. Carbonate intervals where Fe_T is <0.5 wt% are present throughout the Lower Omkyk Member, the late TST of the Upper Omkyk Member, the late TST of the Lower Hoogland Member, and the entire Upper Hoogland Member, and are interpreted to represent probable oxic horizons. Fe-speciation on shales and carbonate rocks indicates oxic conditions in the HST of the Upper Omkyk Member, and in the TST of the Upper Omkyk Member and the lower Hoogland member. Anoxic ferruginous conditions are limited to the early TST of the Upper Omkyk Member and the Lower Hoogland Member, and the HST of the Upper Omkyk Member. Large positive Ce_{SN}/Ce^*_{SN} anomalies [range: 1.06-1.68, average: 1.34±0.21 (1 s.d.)] are observed towards the top of the Lower Omkyk Member in grainstone units (Supplementary Fig 7). Some intermittent, smaller positive anomalies are present towards the top of the Upper Omkyk Member, but the majority of samples show Ce_{SN}/Ce^*_{SN} close to 1 [range: 1.01-1.48, average: 1.18±0.10 (1 s.d.)]. Across all samples the average Y anomaly =71.0, BSI =1.2, Eu/Eu* =1.1 Yb_{SN}/Nd_{SN} =1.1, and ∑REE =2.41ppm.

Driedoornvlagte reef accumulated in a mid-ramp setting, during the TST of the Upper Omkyk Member. The build-up is 7 km wide and a total of 200 m thick: this thickness reflects the incised accommodation space associated with the deeper water setting compared to Zebra River reefs. The build-up is predominantly composed of thrombolitic limestones and grainstones, with

minor dolomitisation. Skeletal animal fossils are abundant, particularly towards the top of the section where *Cloudina* and large *Namapoikia* (up to a meter) are found associated with thrombolites[2,12]. *Namacalathus* is also abundant lower in the section. Large, reef-building *Cloudina hartmannae* (up to 8 mm tube diameter, several cm length) and fissure-inhabiting *Namapoikia* are found towards the top of the section[12,14,15]. Driedoornvlagte has consistently low Fe_T, ranging from 0.03 to 0.07%, and low TOC, ranging from 0.005 to 0.383 wt% (Supplementary Fig 8). This is interpreted to indicate persistently oxic conditions[2]. No bioturbation has been noted, but preservation may be poor in such energetic settings. Bar two negative anomalies (0.88 and 0.86), Driedoornvlagte exhibits Ce_{SN}/Ce^*_{SN} close to unity throughout [range: 0.86-1.14, average: 1.03±0.10 (1 s.d.)] (Supplementary Fig 8). The two negative Ce anomalies are present in samples with superchondritic Y/Ho ratios, but below the >67 threshold we have assigned to screen for clay leaching. We suggest these samples, with higher ∑REE, have been affected by partial leaching of clays, and so the true magnitude of the negative Ce anomalies is likely higher. We include the data in Fig 1 as negative Ce anomalies cannot result from clay or oxide leaching, or alteration, and so likely record original seawater redox conditions [16]. Across all samples the average Y anomaly =75.8, BSI =1.1, Eu/Eu* =1.1 Yb_{SN}/Nd_{SN} =0.96, and ∑REE =0.57ppm.

Brak is a deep water section, which is dominated by fine-grained dolostones inter-bedded with thin sandstones, shales and quartzites indicative of deeper, outer ramp conditions, with shallow subtidal grainstones (limestones) present only towards the very top of the section. There are no animal fossils or

thrombolites present, but some stromatolites occur at approximately 30 m in the Kanies Member[2]. Fe_T is variable, from 0.05 to ~1.89 wt% in the Kanies Member, and from 0.08 to 0.132 in the limestones of the Lower Omkyk Member. Fe-speciation indicates anoxic and ferruginous conditions throughout all carbonates and shales in the Kanies member at Brak[2]. No unequivocal redox proxy data are available for the Lower Omkyk Member as all Fe_T < 0.5 wt%, but TOC is notably >0.5 wt%, ranging from 1.22 to 3.39 wt% (Supplementary Fig 9). Ce_{SN}/Ce^*_{SN} is close to 1.2 throughout, consistent with anoxic conditions, with one notable positive Ce anomaly [range: 0.967-1.530, average: 1.18±0.12 (1 s.d.)] (Supplementary Fig 9). The Y anomaly is notably high in most samples from Brak, average =94.1. The BSI is low =1.1, Yb_{SN}/Nd_{SN} ratios are high (average=1.8), and ∑REE is low (average =0.2 ppm). The Europium anomalies are the largest observed across the basin (range 1.02 - 2.25, average=1.5).

Arasab was deposited in shallow, proximal ramp settings. The base of the section is predominantly composed of limestone units (often displaying evaporitic fabrics) punctuated by thin shale interbeds, transitioning to thick quartzite beds of the Lower Kliphoek Member, followed by interbedded shale and limestone of the Upper Kliphoek Member. The section is capped by a thick limestone unit of the Mooifontein Member, containing distinct oolite bands in the lower reaches. Though the Lower Kliphoek quartzite and Aar Member units are known to contain abundant soft-bodied animal fossils in other localities[17], none have been noted at Arasab[2]. Arasab shows fluctuating anoxia, with anoxic signals in carbonates with high Fe_T interbedded with carbonates with low Fe_T (likely oxic)[2]. Fe_T data from shales range from 0.51 to 0.77wt% and Fe speciation data

indicate fully anoxic ferruginous conditions. Carbonate rocks in the Mara, Kliphoek, and Aar Members have Fe_T > 0.5 wt%, likewise indicating ferruginous conditions. In samples with Fe_T < 0.5 wt%, TOC is low, ranging from 0.05 to 0.13 wt%; these samples are from rocks interbedded with anoxic layers in the Mara and Aar Members, and continuously through the Mooifontein Member, and are taken to indicate sporadic short-lived intervals of probable oxic water column conditions although no bioturbation has been noted. In this locality, REY were only analysed in samples with Fe_T <0.5 wt%, to maximise the proportion of samples that give a non-contaminated signal[16]. Positive Ce anomalies are common, [range: 0.93–1.91, average: 1.28±0.26 (1 s.d.)] with positive anomalies most prevalent in the Upper Kliphoek (Aar) Member, and largely absent in the Mara and Mooifontein Members (Supplementary Fig 10). Several samples show large positive Eu anomalies. Across all samples the average Y anomaly =97.5, BSI =1.2, Eu/Eu* =1.0 Yb_{SN}/Nd_{SN} =1.5, and ∑REE =2.1 ppm.

Grens includes all members of the Dabies Formation of the Kuibis Subgroup. Conglomerates, sandstones and shales dominate the lowermost 20 m, defining the Kanies Member at Grens, with overlying facies of the Mara Member predominantly composed of limestone with shale inter-beds clearly defining patterns of shoaling cyclicity (further evidence from evaporitic fabrics). The Kliphoek Member is composed of limestone with small layers of quartzite, and the capping Aar Member consists of shale, limestone, and dolo-cemented quartzite. At 180 m in-situ assemblages of the Ediacaran fossil *Nemiana* are abundant in coarse sandstone layers[2], for which redox data is not available. Fe_T data was >0.5 wt% for only 17 of the 50 samples analysed, with Fe_{HR}/Fe_T for

these 17 samples indicating anoxic ferruginous conditions. Where Fe_T is <0.5 wt%, TOC is very low, from 0.04 to 0.2 wt%. This is taken as an indication of probable oxic conditions although no bioturbation has been noted, and these horizons are found interbedded with anoxic horizons in the upper Middle and Kliphoek Members. Grens shows positive Ce anomalies as high as 2.15, with highest values in the Kliphoek and Aar Member (Supplementary Fig 11) [range: 1.14–2.15, average: 1.50±0.25 (1 s.d.)]. Only samples with <0.5 wt% Fe_T have been analysed for REY in this section. Across all samples the average Y anomaly =104.6, BSI =1.1, Eu/Eu* =1.1 Yb_{SN}/Nd_{SN} =1.9, and ∑REE =0.9 ppm.

Swartpunt, from the younger Schwarzrand Subgroup, extends close to the Neoproterozoic-Cambrian Boundary and transitions from high-energy inner ramp conditions at the base, followed by a TST, and then shallowing to inner ramp carbonates at the top of the section. At the base of the section, laminated limestone dominates, containing *Namacalathus,* large *Cloudina* and other bioclastic material at some levels. Carbonate microbialites are also found at this level, some with a 'leopardskin' texture. Overlying the limestones are beds of upwards coarsening of green mudstone and to ripple-laminated and thick bedded planar-laminated or cross-bedded sandstones, containing burrows and soft-bodied fossils including *Swartpuntia* and *Pteridinium*[8]. These in turn give way to more thin-bedded limestones and dolomites with dm-scale thrombolites, and thick- and thin-bedded limestones with rare flat-pebble and intraclastic breccias deposited in shallow to sub-tidal ramp settings below storm wave base. These in turn give way to a HST of laminated, flaggy limestones containing small (<5 mm) *Cloudina riemkeae* and thrombolites. Horizontal burrows are first noted

~60 m below the Ediacaran-Cambrian unconformity[18]. All but two of the Fe_T values from Swartpunt carbonates are <0.5 wt%, and these also show consistently low TOC throughout, from 0.04 to 0.07wt% (Supplementary Fig 12). This is taken to indicate oxic conditions, and is confirmed by the presence of complex bioturbation in the upper 60m of the section. TST clastic samples consistently contain Fe_T > 0.5 wt%. Fe_{HR}/Fe_T values vary significantly through the section, but all clastics show an oxic signature. By contrast, two HST carbonate samples with Fe_T > 0.5 wt% occurring some 55 m and 20 m below the Ediacaran-Cambrian unconformity show Fe_{HR}/Fe_T > 0.38, with low Fe_{py}/Fe_{HR} giving an anoxic ferruginous signature. Overall, Fe-speciation suggests persistent oxygenation with two limited anoxic ferruginous horizons[2,19]. Swartpunt carbonates show no positive Ce anomalies (Supplementary Fig 12), which is consistent with well-oxygenated conditions throughout most of Swartpunt. Across all samples the average Y anomaly =69.4, BSI =1.2, Eu/Eu* =1.3, Yb_{SN}/Nd_{SN} =1.1, and ∑REE =2.5 ppm.

The Pinnacle Reefs at Swartkloofberg Farm, southern Namibia, were deposited within TSTs in a mid-ramp setting. They initiated on the flooded surface of the Huns Platform. At the base of the reefs, reef carbonate inter-fingers with siltstones and shales, but the reefs then grew up to 40 m topographic relief above the sea floor. After termination of reef growth, they were enveloped by the shales of the Feldschuhorn Member, of which they now form a part. Mixed communities of skeletal animals of varied sizes persist at the Pinnacle Reefs[2]. The sampled reef was composed predominantly of microbialite, with some laminar micritic layers. Microbialite textures are predominantly stromatolitic at the base (approximately 0–

5m), with thrombolitic textures appearing at approximately 5 m height, and aggregations of Namacalathus (up to 12 mm diameter) becoming more prevalent towards the top of the reef. Carbonate samples from within one of the reefs have low Fe_T with values ranging from 0.042-0.33 wt%, and low TOC, with values ranging from 0.02-0.04 wt%. This is interpreted to indicate oxic conditions. Siliciclastics from nearby Felschuhorn Member (bar one) have Fe_{HR}/Fe_T <0.22, suggesting persistently oxygenated conditions. ∑REE is low for the four carbonates (0.07-0.39), meaning non-normalised HREE concentrations fell below the detection limit. This precludes interpretation of Y anomalies, but La, Ce, Pr and Nd are recorded with sufficient resolution to interpret Ce anomalies for two samples. One negative Ce anomaly (0.53) is recorded, and one other sample shows no anomaly (Supplementary Fig 13).

Supplementary Note 3 – Ce_{SN}/Ce^*_{SN} **cut off values**

Cut-off values used to define negative Ce anomalies are well established (<0.9), but here we report positive Ce anomalies, which have rarely been described from modern or ancient carbonate rocks. We assign a cut off value of >1.3. This is firstly, because we are cautious about interpreting Ce enrichments that are not significant with respect to those observed in modern manganous waters. Secondly, fluctuations in Pr and Nd concentrations, encompassing natural variation and precision during ICP-MS analysis (accurate to within 5%), may result in a calculated Ce anomaly up to 1.2. Because of this, REY patterns need to be screened by eye to show that genuinely anomalous Ce enrichments, relative to the trajectory from the MREE to the LREE, are evident in all samples with

Ce_{SN}/Ce^*_{SN} >1.3 (Supplementary Fig 3). All of our patterns have been additionaly screened to select true Ce enrichments above baseline fluctuations and trends.

We have considered the effect on our data and interpretation of applying a different cut-off, e.g. 1.1 or 1.2. Using a cut-off of >1.3, the total number of samples identified as well-oxygenated was 191; low oxygen, 58; and anoxic, 141. Using a threshold of >1.2 results in 30 samples categorised as oxic switching to manganous, and threshold of >1.1 results in an additional 34 samples switching from oxic to manganous. Some of these environments host small skeletal fossils, and so the total number of small shelly fossils in low oxygen environments would also increase. The pinnacle reefs and Driedoornvlagte, which both foster large skeletal animals and complex, long-lived communities, remain persistently oxic regardless of the cut-off used. We emphasise that where Ce_{SN}/Ce^*_{SN} is between 1.1 and 1.3, no genuine Ce enrichment is observed in REY patterns, and so there is no indication that these samples represent manganous environments (Supplementary Fig 3).

Supplementary note 4 – The role of Fe in Ce cycling

The REY are considered to be scavenged quantitatively onto Fe (oxyhydr)oxides, and fractionated during scavenging onto Mn (oxyhydr)oxides. This is supported by evidence from hydrothermal plumes[20], water column data[21–25], marine Fe-Mn nodules[26], Fe-formation REY data[27] and experimental work[28–31]. However, there is conflicting evidence from the sequential leaching of Fe-Mn nodules that suggests Fe (oxyhydr)oxides may be important in controlling REY fractionation[32,33]. Fe (oxyhydr)oxides may scavenge the middle-REE

preferentially, and exclude Y, but there is only limited evidence that they preferentially accumulate Ce[31,34]. The relative importance of Fe and Mn in controlling Ce oxidation and scavenging is debated, but Mn is generally considered more important for controlling the redox cycling of Ce[20–29].

We assume that Mn (oxyhydr)oxides are the primary carrier for REY in the oceans. If Fe(oxyhydr)oxides were important carriers of Ce, we would anticipate positive Ce anomalies to co-occur with Fe enrichments, but they co-occur with Mn enrichments. Nevertheless, we consider how our interpretation of the data would be affected in the case that Fe (oxyhydr)oxides were important Ce carriers. Firstly, highly reactive Fe enrichments occur in fully anoxic conditions, and so there would be an apparent discrepancy between very low Fe_T and Ce enrichments in the same sample. However, Ce(IV) may undergo reductive dissolution and be released from the surface of Fe (oxyhydr)oxides at a Ce redoxcline independently of other REY. In this case, the carrier phase becomes unimportant, as Ce reduction and release from the surface would occur independently of either Mn or Fe reduction. Further, there is some evidence that Ce(IV) forms a discrete solid oxide phase[34], in which case Ce cycling would occur independently of both Mn and Fe cycling, and at higher oxygen concentrations. However, most evidence supports that Ce fractionation can only occur on the surface of solid Mn (oxyhydr)oxides[33], and therefore tracks Mn redox cycles.

In the Nama Group, we suggest that Mn (oxyhydr)oxides were the main carrier for REY and that the release of excess Ce occurred under manganous conditions. Support for Mn (oxyhydr)oxides as the main carrier phases comes from the

decoupling of Fe and Mn alongside positive Ce anomalies. Mn concentrations may be considerably affected by diagenesis, and so Mn concentration data should be interpreted with caution. Although Mn/Fe ratios are relatively elevated in manganous samples, absolute Mn concentrations and Mn/Sr ratios remain low, consistent with unaltered carbonate.

Supplementary note 5 - Yttrium anomaly thresholds

Positive Ce anomalies occur in samples with seawater features, and similar REY patterns to samples without positive Ce anomalies (Supplementary Fig 3). Although a molar Y/Ho ratio >67 is traditionally used to screen for seawater REY signals[35–37], the interpretation of Y anomalies in our samples is not straightforward, as the dissolution of Mn (oxyhydr)oxides beneath a redoxcline may alter the full REY pattern along with release of excess Ce. Mn (oxyhydr)oxides contain a negative Y anomaly when normalized to ambient waters, but this is not as pronounced as the negative Y anomaly in co-occurring Fe (oxyhydr)oxides[33]. Excess Ce may accumulate beneath a redoxcline via two mechanisms: reduction of Ce(IV) and release from the oxide surface, or reductive dissolution of the Mn (oxyhydr)oxide and release of all oxide bound REY. In the former case, Ce would be enriched in the water without affecting Y. In the latter, redox dissolution may impart a small effect on the Y anomaly. Since the development of Y anomalies is controlled by scavenging onto particles across all depths, including onto Fe (oxyhydr)oxides that would remain intact in a partially oxic manganous zone, excess Y would likely be ubiquitous in the ocean (see data from modern manganous zones with positive Y and Ce anomalies in Fig 1). Further, suspended (oxyhydr)oxide particles in the Rainbow hydrothermal

plumes and ancient Fe-Formations[20,38] exhibit superchondritic Y anomalies, despite their residence time in the water column exceeding experimental constraints on Y equilibration times[28]. This suggests that Mn (oxyhydr)oxides may retain the superchondritic Y anomaly of ambient waters, particularly during rapid precipitation, and yet continue to accumulate Ce in oxic waters. The magnitude of Y anomalies in our samples is controlled by scavenging, reductive dissolution of (oxyhydr)oxides in seawater and any partial clay leaching during acid dissolution[16]. Although the magnitude of the Y anomaly may reduce slightly in seawater in the manganous zone, we do not attempt to interpret the absolute magnitude of Y/Ho, but employ a cut off >67 to exclude samples affected by partial leaching of clay minerals

Supplementary Discussion

Alternative mechanisms for Ce enrichment

Anomalous local REY input

Although REY inputs from rivers or wind blown dust generally carry a flat REY signature[39,40], if terrestrial input was anomalous in the Ediacaran this could explain Ce enrichment in the basin. However, the lack of anomalous Ce behavior in local shales (Supplementary Fig 1 and methods) indicates that the positive Ce anomalies recorded in carbonates cannot be attributed to unusual local REY inputs. Moreover, if positive Ce anomalies resulted from surface maxima[23] we would expect them to be most prevalent in inner ramp sections (Zwartmodder, Arasab and Swartpunt). Although limited Ce enrichments are recorded in these sections, they are more pronounced in deeper inner ramp sections (Zebra River, Omkyk, Grens).

Alkaline waters

Highly alkaline waters in unusual lake settings may exhibit positive Ce anomalies due to stabilization of Ce complexes in the water column[41,42]. There is no evidence that the Nama Group was highly alkaline, and carbon and strontium isotope data both support the Nama Group being normal marine and fully connected to the open ocean[2,43].

Ce oxidation in the presence of siderophores

The presence of Fe-chelating siderophores, such as desferrioxamine B (DFOB), can affect the mobilization of REY during the weathering of igneous rocks [44,45]. This process may affect the input of REY into the basin from terrestrial weathering, but we find no anomalous Ce behavior in terrestrial input (see Methods and Supplementary Fig 1). Further, under Fe-limiting conditions in the water column, microbes release siderophores to scavenge iron from Fe(III) mineral phases, and since Ce-DFOB complexes are orders or magnitude more stable than Ce-carbonate complexes, water column Ce enrichments may occur in unusual environments where siderophore activity is prevalent[46]. However, where bio-available Fe(II) is present in the water column, it is unlikely that siderophores were common. In addition, the presence of siderophores results in enriched Ce alongside extensive La depletion[46], which is in marked contrast to the positive La anomalies observed in the Nama Group.

Reductive dissolution of Fe-Mn (oxyhydr)oxides during diagenesis.

Although seawater REY in carbonate rocks are thought to be preserved during early diagenesis[37], REY released from Fe-Mn (oxyhydr)oxide dissolution in anoxic pore waters could potentially be captured during recrystallization from aragonite to calcite. Modern pore water data rarely show anomalous Ce enrichments[34,47,48], even though Mn (oxyhydr)oxides presumably carry positive Ce anomalies into the sediment[33]. This suggests that there is an additional REY carrier that dominates the REY content of pore waters. One possible candidate is organic matter[34,49], but the REY signal of organic matter is poorly understood, and the low TOC concentrations in most of our samples suggest this was not an important contributor[2]. A more likely candidate is the dissolution of Fe (oxyhydr)oxides.

Pore waters often become fully anoxic within millimeters of the sediment-water interface, and so Mn and Fe (oxyhydr)oxides commonly undergo simultaneous dissolution, or form discrete zones but separated on a cm-scale[50]. If the REY, Fe and Mn in our samples were derived entirely from pore water resetting, the excess Fe over Mn present in all samples would reflect higher Fe contents in the pore waters, as both elements have a partition coefficient close to one [Ref [51]]. Fe (oxyhydr)oxides usually carry an MREE-enriched signal with a negative Y anomaly (similar to shales presented here, Supplementary Fig 1), and this signal would dominate anoxic pore waters[34,52], but this REY pattern is not observed in our carbonate leach, even where Fe concentrations in carbonate are high. This argues against destruction of seawater REY patterns via incorporation of pore water REY. However, in the water column, Mn (oxyhydr)oxide dissolution can occur in the absence of Fe (oxyhydr)oxide dissolution, in a stable meter -

decimeter thick manganous zone. A water column origin for carbonate-bound REY is the only way to account for the relatively enriched Mn/Fe ratios, but with higher absolute Fe concentrations, and positive Ce anomalies alongside superchondritic Y anomalies.

REY concentrations in pore waters are an order of magnitude higher than in seawater, and the REY content of carbonates should increase during diagenetic exchange, alongside increases in Fe and Mn contents. But positive Ce anomalies correlate with lower ∑REE, [Fe] and [Mn] (Supplementary Fig 2). Because positive Ce anomalies do not correlate with diagenetic proxies (low $\delta^{18}O_{carb}$, high Mn/Sr), or with proxies for other forms of potential contamination (low Y/Ho, high Fe or Mn concentrations etc.), but instead with stratigraphic trends, we can rule out wholesale diagenetic exchange of REY as a primary control.

Diffusion from reducing inshore sediments into seawater

Mobilization of Ce from reducing inshore sediments[53] may explain local Ce peaks, but Ce is rapidly oxidized in overlying oxic waters. The positive Ce reported here occurs in sediments with low TOC and oxic Fe-speciation signals[2]. If excess Ce originates from diffusion above reducing seafloor sediments, we would expect the Ce anomalies to peak in anoxic waters, but instead, they are observed predominantly in oxic waters.

Supplementary References

1. Pourmand, A., Dauphas, N. & Ireland, T. J. A novel extraction chromatography and MC-ICP-MS technique for rapid analysis of REE, Sc and Y: Revising CI-chondrite and Post-Archean Australian Shale (PAAS) abundances. *Chemical Geology* **291,** 38–54 (2012).
2. Wood, R. A. *et al.* Dynamic redox conditions control late Ediacaran ecosystems in the Nama Group, Namibia. *Precambrian Research* **261,** 252–271 (2015).
3. Saylor, B. Z., Grotzinger, J. P. & Germs, G. J. B. Sequence stratigraphy and sedimentology of the Neoproterozoic Kuibis and Schwarzrand Subgroups (Nama Group), southwestern Namibia. *Precambrian Research* **73,** 153–171 (1995).
4. Saylor, B. Z., Kaufman, A. J., Grotzinger, J. P. & Urban, F. A Composite Reference Section for Terminal Proterozoic Strata of Southern Namibia. *SEPM Journal of Sedimentary Research* **68,** (1998).
5. Germs, G. J. B. Implications of a sedimentary faceis and depositional environmental analysis of the Nama group in South West Africa/Namibia. *Geological Society of South Africa* **11,** 89–114 (1983).
6. Germs, G. J. B. The Neoproterozoic of southwestern Africa, with emphasis on platform stratigraphy and paleontology. *Precambrian Research* **73,** 137–151 (1995).
7. Grotzinger, J. P., Bowring, S. A., Saylor, B. Z. & Kaufman, A. J. Biostratigraphic and Geochronologic Constraints on Early Animal Evolution. *Science* **270,** 598 –604 (1995).

8. Narbonne, G. M., Saylor, B. Z. & Grotzinger, J. P. The youngest Ediacaran fossils from southern Africa. *Journal of Paleontology* **71.06,** 953–967 (1997).
9. Germs, G. J., Knoll, A. H. & Vidal, G. Latest Proterozoic microfossils from the Nama Group, Namibia (South West Africa). *Precambrian Research* **32,** 45–62 (1986).
10. Grant, S. W. Shell structure and distribution of Cloudina, a potential index fossil for the terminal Proterozoic. *Am J Sci* **290-A,** 261–294 (1990).
11. Grotzinger, J. P., Watters, W. A. & Knoll, A. H. Calcified metazoans in thrombolite-stromatolite reefs of the terminal Proterozoic Nama Group, Namibia. *Paleobiology* **26,** 334 –359 (2000).
12. Wood, R. A., Grotzinger, J. P. & Dickson, J. A. D. Proterozoic Modular Biomineralized Metazoan from the Nama Group, Namibia. *Science* **296,** 2383 –2386 (2002).
13. Macdonald, F. A., Pruss, S. B. & Strauss, J. V. Trace fossils with spreiten from the late Ediacaran Nama Group,Namibia: complex feeding patterns five million years before the Precambrian–Cambrian boundary. *Journal of Paleontology* **88,** 299–308 (2014).
14. Penny, A. *et al.* Ediacaran metazoan reefs from the Nama Group, Namibia. *Science* **344,** 1504–1506 (2014).
15. Wood, R. & Curtis, A. Extensive metazoan reefs from the Ediacaran Nama Group, Namibia: the rise of benthic suspension feeding. *Geobiology* **13,** 112–122 (2015).
16. Tostevin, R. *et al.* Effective use of cerium anomalies as a redox proxy in carbonate-dominated marine settings. *Chemical Geology* **438,** 146–162 (2016).

17. Hall, M. *et al.* Stratigraphy, palaeontology and geochemistry of the late Neoproterozoic Aar Member, southwest Namibia: Reflecting environmental controls on Ediacara fossil preservation during the terminal Proterozoic in African Gondwana. *Precambrian Research* **238,** 214–232 (2013).
18. Jensen, S. & Runnegar, B. N. A complex trace fossil from the Spitskop Member (terminal Ediacaran–? Lower Cambrian) of southern Namibia. *Geological Magazine* **142,** 561–569 (2005).
19. Darroch, S. A. F. *et al.* Biotic replacement and mass extinction of the Ediacara biota. *Proc. R. Soc. B* **282,** 1814 (2015).
20. Edmonds, H. N. & German, C. R. Particle geochemistry in the Rainbow hydrothermal plume, Mid-Atlantic Ridge. *Geochimica et Cosmochimica Acta* **68,** 759–772 (2004).
21. de Baar, H. J. ., German, C. R., Elderfield, H. & van Gaans, P. Rare earth element distributions in anoxic waters of the Cariaco Trench. *Geochimica et Cosmochimica Acta* **52,** 1203–1219 (1988).
22. De Carlo, E. H. & Green, W. J. Rare earth elements in the water column of Lake Vanda, McMurdo Dry Valleys, Antarctica. *Geochimica et Cosmochimica Acta* **66,** 1323–1333 (2002).
23. Moffett, J. W. Microbially mediated cerium oxidation in sea water. *Nature* **345,** 421–423 (1990).
24. Sholkovitz, E. R., Landing, W. M. & Lewis, B. L. Ocean particle chemistry: The fractionation of rare earth elements between suspended particles and seawater. *Geochimica et Cosmochimica Acta* **58,** 1567–1579 (1994).
25. German, C. R. & Elderfield, H. Rare earth elements in the NW Indian Ocean. *Geochimica et Cosmochimica Acta* **54,** 1929–1940 (1990).

26. De Carlo, E. R. Rare earth element fractionation in hydrogenetic Fe-Mn crusts: The influence of carbonate complexation and phosphatization on Sm/Yb ratios. *Society for Sedimentary Geology* **66**, 271-285 (2000).
27. Planavsky, N. *et al.* Rare Earth Element and yttrium compositions of Archean and Paleoproterozoic Fe formations revisited: New perspectives on the significance and mechanisms of deposition. *Geochimica et Cosmochimica Acta* **74,** 6387–6405 (2010).
28. Bau, M. Scavenging of dissolved yttrium and rare earths by precipitating iron oxyhydroxide: experimental evidence for Ce oxidation, Y-Ho fractionation, and lanthanide tetrad effect. *Geochimica et Cosmochimica Acta* **63,** 67–77 (1999).
29. Ohta, A. & Kawabe, I. REE (III) adsorption onto Mn dioxide (MnO_2) and Fe oxyhydroxide: Ce (III) oxidation by MnO_2. *Geochimica et Cosmochimica Acta* **65,** 695–703 (2001).
30. Koeppenkastrop, D. & De Carlo, E. H. Sorption of rare-earth elements from seawater onto synthetic mineral particles: An experimental approach. *Chemical Geology* **95,** 251–263 (1992).
31. Quinn, K. A., Byrne, R. H. & Schijf, J. Sorption of yttrium and rare earth elements by amorphous ferric hydroxide: Influence of solution complexation with carbonate. *Geochimica et Cosmochimica Acta* **70,** 4151–4165 (2006).
32. Bau, M. & Koschinsky, A. Oxidative scavenging of cerium on hydrous Fe oxide: evidence from the distribution of rare earth elements and yttrium between Fe oxides and Mn oxides in hydrogenetic ferromanganese crusts. *Geochemical Journal* **43,** 37–47 (2009).

33. Bau, M. *et al.* Discriminating between different genetic types of marine ferro-manganese crusts and nodules based on rare earth elements and yttrium. *Chemical Geology* **381,** 1–9 (2014).
34. Haley, B. A., Klinkhammer, G. P. & McManus, J. Rare earth elements in pore waters of marine sediments. *Geochimica et Cosmochimica Acta* **68,** 1265–1279 (2004).
35. Ling, H.-F. *et al.* Cerium anomaly variations in Ediacaran–earliest Cambrian carbonates from the Yangtze Gorges area, South China: implications for oxygenation of coeval shallow seawater. *Precambrian Research* **225,** 110–127 (2013).
36. Nothdurft, L. D., Webb, G. E. & Kamber, B. S. Rare earth element geochemistry of Late Devonian reefal carbonates, Canning Basin, Western Australia: confirmation of a seawater REE proxy in ancient limestones. *Geochimica et Cosmochimica Acta* **68,** 263–283 (2004).
37. Webb, G. E. & Kamber, B. S. Rare earth elements in Holocene reefal microbialites: a new shallow seawater proxy. *Geochimica et Cosmochimica Acta* **64,** 1557–1565 (2000).
38. Slack, J., Grenne, T., Bekker, A., Rouxel, O. & Lindberg, P. Suboxic deep seawater in the late Paleoproterozoic: evidence from hematitic chert and iron formation related to seafloor-hydrothermal sulfide deposits, central Arizona, USA. *Earth and Planetary Science Letters* **255,** 243–256 (2007).
39. Goldstein, S. J. & Jacobsen, S. B. Rare earth elements in river waters. *Earth and Planetary Science Letters* **89,** 35–47 (1988).

40. Greaves, M. J., Statham, P. J. & Elderfield, H. Rare earth element mobilization from marine atmospheric dust into seawater. *Marine Chemistry* **46,** 255–260 (1994).
41. Johannesson, K. H., Lyons, W. B. & Bird, D. A. Rare earth element concentrations and speciation in alkaline lakes from the western U.S.A. *Geophys. Res. Lett.* **21,** 773–776 (1994).
42. Möller, P. & Bau, M. Rare-earth patterns with positive cerium anomaly in alkaline waters from Lake Van, Turkey. *Earth and Planetary Science Letters* **117,** 671–676 (1993).
43. Kaufman, A. J., Jacobsen, S. B. & Knoll, A. H. The Vendian record of Sr and C isotopic variations in seawater: Implications for tectonics and paleoclimate. *Earth and Planetary Science Letters* **120,** 409–430 (1993).
44. Bau, M., Tepe, N. & Mohwinkel, D. Siderophore-promoted transfer of rare earth elements and iron from volcanic ash into glacial meltwater, river and ocean water. *Earth and Planetary Science Letters* **364,** 30–36 (2013).
45. Kraemer, D., Kopf, S. & Bau, M. Oxidative mobilization of cerium and uranium and enhanced release of 'immobile' high field strength elements from igneous rocks in the presence of the biogenic siderophore desferrioxamine B. *Geochimica et Cosmochimica Acta* **165,** 263–279 (2015).
46. Kraemer, S. M. Iron oxide dissolution and solubility in the presence of siderophores. *Aquat. Sci.* **66,** 3–18 (2004).
47. Abbott, A. N., Haley, B. A., McManus, J. & Reimers, C. E. The sedimentary flux of dissolved rare earth elements to the ocean. *Geochimica et Cosmochimica Acta* **154,** 186–200 (2015).

48. Soyol-Erdene, T.-O. & Huh, Y. Rare earth element cycling in the pore waters of the Bering Sea Slope (IODP Exp. 323). *Chemical Geology* **358,** 75–89 (2013).
49. Freslon, N. *et al.* Rare earth elements and neodymium isotopes in sedimentary organic matter. *Geochimica et Cosmochimica Acta* **140,** 177–198 (2014).
50. Froelich, P. N. *et al.* Early oxidation of organic matter in pelagic sediments of the eastern equatorial Atlantic: suboxic diagenesis. *Geochimica et Cosmochimica Acta* **43,** 1075–1090 (1979).
51. Dromgoole, E. L. & Walter, L. M. Iron and manganese incorporation into calcite : effects of growth kinetics, temperature and solution chemistry. *Chemical geology* **81,** 311–336 (1990).
52. Bayon, G. *et al.* Evidence for intense REE scavenging at cold seeps from the Niger Delta margin. *Earth and Planetary Science Letters* **312,** 443–452 (2011).
53. De Baar, H. J. W., Bacon, M. P. & Brewer, P. G. Rare-earth distributions with a positive Ce anomaly in the Western North Atlantic Ocean. *Nature* **301,** 324–327 (1983).